8-2012

Multi-Functional Reconfigurable Antenna Development by Multi-Objective Optimization

Xiaoyan Yuan
Utah State University

MULTI-FUNCTIONAL RECONFIGURABLE ANTENNA DEVELOPMENT BY MULTI-OBJECTIVE OPTIMIZATION

by

Xiaoyan Yuan

A dissertation submitted in partial fulfillment
of the requirements for the degree

of

DOCTOR OF PHILOSOPHY

in

Electrical Engineering

Approved:

Dr. Bedri A. Cetiner Major Professor	Dr. Doran J. Baker Committee Member
Dr. Jacob Gunther Committee Member	Dr. Edmund Spencer Committee Member
Dr. T.C. Shen Committee Member	Dr. Mark R. McLellan Vice President for Research and Dean of the School of Graduate Studies

UTAH STATE UNIVERSITY
Logan, Utah

2012

Abstract

Multi-Functional Reconfigurable Antenna Development by Multi-Objective Optimization

by

Xiaoyan Yuan, Doctor of Philosophy

Utah State University, 2012

Major Professor: Dr. Bedri A. Cetiner
Department: Electrical and Computer Engineering

This dissertation work builds upon the theoretical and experimental studies of radio frequency micro- and nano-electromechanical systems (RF M/NEMS) integrated multi-functional reconfigurable antennas (MRAs). This work focuses on three MRAs with an emphasis on a wireless local area network (WLAN), 5-6 GHz, beam tilt, and polarization reconfigurable parasitic layer-based MRA with inset micro-strip feed. The other two antennas are an X band (8-12 GHz) beam steering MRA with aperture-coupled micro-strip fed and wireless personal area network (WPAN), 60 GHz, inset micro-strip fed MRA for dual frequency and dual polarization operations. For the WLAN (5-6 GHz) MRA, a detailed description of the design methodology, which is based on the joint utilization of electromagnetic (EM) full-wave analysis and multi-objective genetic algorithm, and fundamental theoretical background of parasitic layer-based antennas are given. Various prototypes of this MRA have been fabricated and measured. The measured and simulated results for both impedance and radiation characteristics are given. The work on the MRAs operating in the X band and 60 GHz region focuses on the theoretical aspects of the designs. Different than the WLAN MRA, which uses inset fed structure, the aperture-coupled feed mechanism has been investigated with the goal of improving the bandwidth and beam-tilt capabilities

of these MRAs. The simulated results are provided and the working mechanisms are described. The results show that the aperture-coupled feed mechanism is advantageous both in terms of enhanced bandwidth and beam-steering capabilities. Finally, this dissertation work concludes with plans for future work, which will build upon the findings and the results presented herein.

(80 pages)

Public Abstract

Multi-Functional Reconfigurable Antenna Development by Multi-Objective Optimization

by

Xiaoyan Yuan, Doctor of Philosophy

Utah State University, 2012

Major Professor: Dr. Bedri A. Cetiner
Department: Electrical and Computer Engineering

Antennas are the most essential and significant elements of any wireless communication system. The most common antennas used in wireless communication systems include dipoles/monopoles, horn antennas, loop antennas, and micro-strip antennas. Each type possesses inherent advantages and disadvantages that make them satisfactory for particular applications. The properties of these antennas, however, are fixed by the initial design and cannot be changed. These fixed properties impose restrictions on the overall system performance as the antenna cannot adapt its characteristics in response to the changing propagation parameters of the wireless medium. A reconfigurable antenna, on the other hand, can dynamically change its properties in frequency, polarization, and radiation pattern, and therefore it can adapt its behavior to a winning set of parameters for a given propagation environment. For example, single antennas typically used in a cellular telephone are monopole or micro-strip-based antennas and may or may not have multi-frequency capabilities. The ability to tune the antenna's operating frequency could be utilized to change operating bands, filter out interfering signals, or tune the antenna to operate in a new environment. If the antenna's radiation pattern could be changed, it could be redirected toward the access point and use less power for transmission, resulting in a valuable saving in battery power. However, the development of these multi-functional antennas poses some challenges. These

challenges lie not only in obtaining the desired levels of antenna functionality but also in the implementation of the antenna.

This dissertation work builds upon the theoretical and experimental studies of a single reconfigurable antenna, which could deliver the same functionality of more than one traditional single-function antennas. A single reconfigurable antenna element is named multi-functional reconfigurable antenna (MRA). This work focuses on three specific MRAs with an emphasis on a wireless local area network (WLAN), beam tilt, and polarization reconfigurable parasitic layer-based MRA with inset micro-strip feed. The other two antennas are, an X band beam steering MRA with aperture-coupled micro-strip feed and wireless personal area network (WPAN), inset micro-strip fed MRA for dual frequency and dual polarization operations. For the WLAN MRA, a detailed description of the design methodology, which is based on the joint utilization of electromagnetic (EM) full-wave analysis and multi-objective genetic algorithm, is given. Fundamental theoretical background of parasitic layer-based antennas is also investigated in detail. Various prototypes of this MRA have been fabricated and measured. The measured and simulated results for both impedance and radiation characteristics are given. The work on the MRAs operating in the X band and 60 GHz WPAN focuses on the theoretical aspects of the designs. Different than the WLAN MRA, which uses inset fed structure, the aperture-coupled feed mechanism has been investigated with the goal of improving the bandwidth and beam-tilt capabilities of these MRAs. The simulated results are provided and the working mechanisms are described. The results show that the aperture-coupled feed mechanism is advantageous both in terms of enhanced bandwidth and beam-steering capabilities. Finally, this work concludes with the plans for future work which will build upon the finding and results presented herein.

To my grandfather Kun, my father Houqiang, my mother Suli, and my husband Xing
I can't do it without your love...

Acknowledgments

My upmost gratitude goes to my major professor, Dr. Bedri A. Cetiner, for allowing me to join his group, for his expertise and kindness, and for his support and guidance throughout the project. I believe that one of the main gains of this program was working with Dr. Cetiner and gaining his trust and friendship. My thanks and appreciation go to my committee members, Dr. Baker, Dr. Gunther, Dr. Spencer, and Dr. Shen. I owe a lot to my friends and colleagues, the visiting professor Dr. Oguz Kaynar, and others in our research team. Our conversations and work together have greatly helped me on the research work.

Xiaoyan Yuan

Contents

List of Tables

List of Figures

Acronyms

MRA	multi-functional reconfigurable antenna
MIMO	multiple-input multiple-output
BER	bit error rate
EM	electromagnetic
WLAN	wireless local area network
MEMS	micro electro mechanical system
RF	radio frequency
GA	genetic algorithm
AL	aluminum
TaN	tantalum nitrite
HIEM	high impedance electromagnetic surface
NSGA	non-dominate sorting genetic algorithm
NSGA-II	improved version of non-dominate sorting genetic algorithm
BW	bandwidth
AR	axial ratio
VSWR	voltage standing wave ratio
ITU	International Telecommunications Union
DSN	Deep Space Network
EPR	electron paramagnetic resonance
BCB	benzocyclobutene
PDMS	polydimethylsiloxane
PAN	personal area network
WPAN	wireless personal area network
IrDA	infrared data association
CPW	coplanar waveguide
GSG	ground signal ground
MMIC	microwave monolithic integrated circuit

DC	direct current
TM	transverse magnetic
GHz	gigahertz
VNA	vector network analyzer

Chapter 1

Introduction and Motivation

As the next generation wireless communications systems require to support multi-mode and multi-band applications, the number of antenna elements on these platforms increases. This, in turn, causes problems associated with co-site interference, cost, maintainability, reliability, and increased weight. One approach to alleviate such challenges is to use a multi-function reconfigurable antenna which can replace multiple of single function legacy antennas. This is the main reason for the recent popularity of multi-functional reconfigurable antennas (MRAs) [1, 2].

An MRA is a single antenna element which could perform multiple functions by dynamically changing its properties (frequency, radiation pattern and polarization) [3, 4]. The reconfigurability may be achieved by using radio frequency (RF) micro electro mechanical system (MEMS) or other developing technologies such as liquid metal systems [5]. For example, an MRA can operate over several frequency bands simultaneously or operate over a wide band instantaneously [6–8]. It can also form a desired radiation pattern or steer the beam into different directions [9, 10]. The polarization of a specific beam direction could also be reconfigured between linear and circular polarizations [11]. All the above benefits can result in a significant reduction in the overall size of multi-mode multi-band wireless communication systems by replacing multiple single-function legacy antennas. Also, the reconfigurable antenna properties of an MRA can be used as important additional degrees of freedom in an adaptive wireless communication system. One example is multi-input multi-output (MIMO) systems equipped with MRAs. Such a system attains improved channel diversity performance which results in a robust and reliable wireless communications. This is due mainly to the additional degree of freedom provided by an MRA which enables further exploitation of the theoretical gains of MIMO systems [12]. The capacity of a MIMO

wireless communication with a sparse multi-path structure could also be maximized by reconfigurable antenna arrays [13]. Reconfigurable radiation pattern of a MRA with different degrees of pattern diversity can be used to improve link capacity for MIMO communication systems [14]. The system equipped with reconfigurable antennas could select the optimal radiation state in response to the changes in the propagation environment, where the receive signal-to-noise ratio (SNR) is maximized [15]. Likewise, radiation patterns of MRA can be used to quantify the communication link performance gains by choosing the mode which maximizes capacity and minimizes bite error rate (BER) [9]. A substantial performance gain is achievable with the proposed system because of the capability of polarization diversity provided by the MRA. In particular, it was shown that an adaptive MIMO wireless communication system equipped with MRA array can provide gains up to 30 dB as compared to conventional fixed MIMO systems [16]. All these additional benefits result from the joint optimization of dynamically reconfigurable antenna properties with adaptive space-time modulation techniques in response to the changes in the propagation environment [17].

In order to dynamically change the properties of a MRA, the current distribution over the volume of the antenna needs to be changed, where each distribution corresponds to a different mode of operation. To the end, the reconfiguration mechanisms may be classified under three categories [5]. First group consists of discrete elements such as RF-switches [2, 3, 18–22] and varactors [8, 23]. These elements can be integrated within the MRA structure to change the geometry by switching among various geometrical portions that make up the MRA and the feed circuitry. Second, tunable materials can be used as MRA substrate, where the variation of the permeability of this substrate enables to tune the operating frequency of the antenna [24]. Finally, reconfiguration can be achieved by using the mechanical movement of RF MEMS type switches [25–28]. This option is very attractive due mainly to the monolithic integration capability of RF MEMS with antenna segments, but it has some drawbacks such as the reliability problems associated with micro mechanical actuation.

In this dissertation, parasitic layer-based reconfiguration approach is introduced and its working mechanism is also comprehensively presented. The modeling of MRAs design, fabrication and characterization of prototypes are provided. There are some significant advantages for the parasitic layer-based reconfiguration method. First, MEMS switch is chosen for its monolithic integration capability with antenna segments along with low loss properties [23]. Second, separation of driven patch antenna element and parasitic pixels eases the burden on the implementation of both design and fabrication. When MRA is operated to provide small number of modes of operations, both design and fabrication may be simple. This is due to the small number of interconnecting switches, i.e., 3-5 switches, required to provide the multi functions. For example, the dual frequency or dual polarization MRA for WPAN, which are studied in this work, has two modes of operations. When MRA is designed to operate for large number of modes of operations, it becomes extremely challenging to accommodate a great number of switches along with the associated control circuitry without harming the antenna performances. The MRA for WLAN applications constitute the core of this work. This MRA has six modes of operations for the beam steering as well as polarization shifting. Therefore, a novel reconfiguration approach must be followed to avoid the implementation challenges. The other MRAs studied in this work are an X band MRA and 60 GHz WPAN MRA of which modes of operations are limited to three. In conventional designs of MRA, the switching network is integrated within the same surface layer of driven antenna element [1–4]. The approach adopted in this work differs from the conventional approach, where the module responsible for the reconfigurable modes of operations is separated from the driven antenna. This module consists of a number of metallic rectangular-shaped electrically small parasitic pixels along with the associated controlling network. Not having a physical conductive connection between driven antenna element and reconfigurable parasitic layer provides the following advantages: 1) MEMS switches are exposed to small amount of RF power, thereby the problems associated with limited power handling capabilities are alleviated; 2) The mutual coupling effects between the active antenna element and MEMS part, which may be deleterious to the MRA per-

formance, are minimized and can be better controlled owing to these separate layers; 3) These layers can be designed and fabricated separately without imposing design constraints on each other, where optimum individual designs can be achieved for the best overall system level performance. In addition, there is no constraint on the distance between driven antenna and reconfigurable parasitic layer. The distance can be simply chosen to be the standard thickness of the RF compatible substrate yielding a small size compact structure. In the previous works, this distance is typically chosen to be $\lambda/4$, to obtain a good impedance match [29], which results in a bulky structure.

In a typical MRA design, such as MRA patch for WLAN applications studied in this dissertation research, Electromagnetic (EM) interactions within the antenna architecture occur in two fashions. The first one is the EM mutual coupling that takes place between active and passive (disconnected) parts of the MRA [30]. As is well known, when a parasitic element is placed in close proximity to an active element, a current is induced in the parasitic element by mutual coupling that in return changes the input impedance and radiation characteristics of the antenna. Second interaction occurs between monolithically integrated RF M/NEMS and antenna segments [3, 21, 22]. Therefore in this work, special efforts were concentrated on the investigations on the combination of these two interaction mechanism. This is critical in order to design MRAs with optimum dimensions and architectures yileding higher gain and increased operational bandwidth [31–33].

An efficient feeding mechanism of an antenna is critically important in achieving an antenna design with optimized performance characteristics. The very first consideration for feeding selection is an efficient transfer of power between the radiating structure and feed structure, that is, impedance matching between the two [34]. There are several basic types of feeding techniques: micro-strip feed, coaxial feed, CPW feed, and aperture-coupled feed, which will be simply explained in Appendix A. For a given set of performance metrics, the proper feeding mechanism must be chosen. The mechanism of micro-strip feed is to transmit the energy directly from source into antenna through micro-strip line. For aperture-coupled feed, energy is coupled from feed to the driven antenna element through

aperture. We determined that for the X band beam steering MRA, aperture-coupled feed is more advantageous than the inset micro-strip feed in terms of wider common bandwidth, larger beam steering, and higher realized gain on each beam direction. As the MRA is desired to work with large number modes of operations, an efficient design methodology must be followed for selecting out the best solutions. Multi-objective genetic algorithm (GA) has been widely used to solve types of EM engineering problems, including parameter optimizations of different types of antenna designs [35, 36], antenna arrays [10, 37–40], filter [41], and microwave absorber designs [42–45]. It is proven to be a useful option for dealing with design which has more than one aim conflicting each other. For the WLAN MRA that has six modes of operations, three objectives includes required realized gain in three directions of arrival, desired bandwidth, and targeted polarization types.

In addition to adopting an optimum geometrical design, it is also critically important to follow an efficient design methodology, when MRA is intended to work with a large number of modes of operations. Multi-objective genetic algorithm (GA) has been widely used to solve various types of EM engineering problems, i.e., parameter optimizations of antenna designs [35,36], antenna arrays [10,37–40], filter [41], and microwave absorb designs [42–45]. It is proven to be a useful option for dealing with design which has more than one aim conflicting each other. For the design of wireless local area network (WLAN) MRA, which has six modes of operations, there are three objectives: required realized gain in three beam directions, desired bandwidth, and targeted polarization types. Therefore for this design, Matlab GA direct toolbox and full wave EM analysis tools based on the finite element method (Ansys HFSS [46]), are jointly used to solve the optimization problem. Communication between Matlab and HFSS is implemented through the Matlab-API (Application Program Interface). Matlab GA creates script file for a given configuration. HFSS loads this file and runs a full wave simulation to create the reports. Matlab GA reads these reports and calculates fitness values for solutions. Besides, EM analysis tool based on method of moment (ADS momentum) is used to calculate basic parameters of driven antenna element to carry out EM simulations. The designs of MRAs using M/NEMS switches as building

blocks including the bias circuitry are performed through these simulations. MRA with six modes of operation for WLAN has been fabricated and the measurement results of prototypes are provided together with the simulation ones. This work has provided the complete designs of the beam steering MRA for X band. In the future work, these results will be used for fabrication with the goal of characterizing various prototypes. The simulated results of dual frequency or dual polarization MRAs for wireless personal area network (WPAN) will be used to optimize the position and the number of the switches for optimal performances, i.e., S-parameters and the axial ratio (AR) value on the beam direction with maximum realized gain.

The rest of the dissertation is organized as follows: Chapter 2 describes the details of architecture and working mechanism of the parasitic layer based MRA for WLAN. Chapter 3 focuses on the design and optimization methodology with an emphasis on the multi-objective genetic algorithm. Chapter 4 presents the simulated results for various modes of operation along with measured results obtained from a group of prototype MRAs. Chapter 5 demonstrates the design work on the X band beam steering MRAs along with the discussion on feeding techniques of antenna. Simulated results of two types of feed are exhibited and compared. Chapter 6 deals with 60 GHz WPAN MRA designs with simulated results on impedance and radiation characteristics provided. Eventually, the dissertation is concluded in Chapter 7, where the future work plan is also included.

Chapter 2

Parasitic Layer-Based Reconfigurable Antenna Design

2.1 Introduction

A parasitic layer-based multi-functional reconfigurable antenna (MRA) design based on multi-objective genetic algorithm optimization used in conjunction with full-wave EM analysis is presented. The MRA is capable of steering its beam into three different directions ($\theta_i = -30^o, 0^o, 30^o$) simultaneously with polarization reconfigurability ($P_j = Linear, Circular$) having six different modes of operation. The MRA consists of a driven micro-strip fed patch element and a reconfigurable parasitic layer, and is designed to be compatible with IEEE-802.11 WLAN standards (5-6 GHz range). The parasitic layer is placed on top of the driven patch. The upper surface of the parasitic layer has a grid of 5×5 electrically small rectangular-shaped metallic pixels, i.e., reconfigurable parasitic pixel surface. The EM energy from the driven patch element couples to the reconfigurable parasitic pixel surface by mutual coupling. The adjacent pixels are connected/disconnected by means of switching, thereby changing the geometry of pixel surface, which in turn changes the current distribution over the parasitic layer, results in the desired mode of operation in beam direction and polarization.

A prototype of the designed MRA has been fabricated on quartz substrate. The results from simulations and measurements agree well indicating ∼8 dB gain in all modes of operation.

As the existing wireless networks keep buckling under the increasing demand for high data rates, the research and development efforts focusing on MRAs also keep gaining significant interest [1–4,6,9,12–16]. Despite the conceptual simplicity of MRAs, their designs and implementations pose some serious challenges in terms of design techniques and fabrication technology. This is, in particular, the case when an MRA has a large number of modes

of operation such as the one presented in this dissertation, where there are six modes of operation corresponding to three beam directions ($\theta_i = -30^o, 0^o, 30^o$) and two polarizations ($P_j = Linear, Circular$). The majority of MRAs that have been presented thus far integrate the switching network (individual switches and control circuitry) within the driven antenna region [1–4]. Although this might be a viable option for MRAs with little number of interconnecting switches, i.e., ∼3-5 switches, it becomes extremely challenging to accommodate a large number of switches along with the associated control circuitry without harming the antenna performances. In this dissertation, we present a new reconfiguration technique, where the reconfigurability in antenna properties is achieved by coupling the electromagnetic (EM) energy from the driven antenna to a reconfigurable parasitic layer by means of EM mutual coupling. This parasitic layer of which upper surface contains a grid of 5×5 electrically small metallic rectangular-shaped pixels, namely "reconfigurable parasitic pixel surface," is placed on top of the active antenna. The reconfigurable parasitic pixel surface and the active antenna region are separated from each other in the sense that there is no physical conductive connection between them. The pixels of the reconfigurable pixel surface are interconnected by MEMS type switches. Judicious activation of the switches changes the upper surface geometry of the parasitic layer, which in turn results in the desired mode of operation. This reconfiguration approach provides significant advantages both in terms of design and fabrication: 1) the switch of choice for MRAs has mainly been the MEMS switch due to monolithic integration capability with antenna segments along with its low loss characteristics [47]. The main disadvantage on the other hand is the RF power handling capability. In our design, this drawback is alleviated as the switches, which are separated from the driven antenna, get exposed to only a minor portion of the RF power available on the driven antenna surface. 2) The design constraints imposed on the driven antenna and the switching circuitry by each other are removed. Therefore, they can be designed separately enabling to choose the optimum individual designs that best meet the overall system level performance requirements. As the bias circuitry and the switches are separated from the driven antenna, any deleterious coupling effect that may disturb the

MRA performance is also minimized. 3) Finally, the fabrication of the antenna becomes easier as the switching part can be fabricated separately and be simply assembled together with the driven antenna. It is also worth noting that there is no constraint on the distance from driven antenna to the reconfigurable pixel surface, which is simply be chosen to be the thickness of MEMS compatible quartz substrate (0.525 mm). In order to ensure a good impedance match, this distance must typically be $\sim\lambda/4$ for the previous work on antennas with parasitic elements [18, 19, 29, 48–50] resulting in bulky structures.

Given the large number of modes of operation of the presented MRA, one must follow an efficient design methodology. To this end, we employed multi-objective genetic algorithm (GA) optimization in conjunction with full-wave analysis. The GA is an artificial intelligence procedure based on the theory of natural selection and evolution. It uses the idea of survival of the fittest by progressively accepting better solutions to the problems. GA differs from conventional nonlinear optimization techniques in that, it searches by maintaining a population of solutions, from which, better solutions are created rather than making incremental changes to a single solution to the problem. It has recently been gaining popularity in solving EM and antenna problems which are complex and numerically intensive, include nonlinear relationships and need exhaustive search in a wide solution space, which all apply to the presented MRA design.

2.2 Antenna Architecture and Working Mechanism

2.2.1 Structure

The 3D schematic of the MRA, namely "MRA parasitic" with critical design parameters is shown in Fig. 2.1. It consists of two layers, namely patch and parasitic layers. The patch layer ($60\times60\times1$ mm^3), which is built by a quartz substrate (ϵ_r=3.9, tanδ=0.0002) [51], contains the driven patch antenna element and portions of the highly resistive bias lines. These lines, through which the DC control voltages for MEMS actuation are applied, starts running from the MEMS switch locations on the parasitic layer to the bias pads located on the patch layer as shown in Fig. 2.1. The transition of the highly resistive bias lines from

the parasitic layer to the patch layer is accomplished by using wedge type of aluminum (Al) wire bonds with a diameter of 0.025 mm. The choice of quartz substrate is due to its good RF properties and MEMS process compatibility. The standard driven patch antenna is designed to operate at ∼5.2 GHz and is fed by a micro-strip feed line of 50Ω characteristic impedance. The parasitic layer ($32\times24\times0.525$ mm^3) is placed on top of the patch layer. The upper surface of the parasitic layer has a grid of 5×5 rectangular-shaped metallic pixels, i.e., reconfigurable parasitic pixel surface, with individual pixel size being 4.8×3.6 mm^2, interconnecting MEMS switches, and highly-resistive DC bias lines as shown in Fig. 2.1. The vertical distance from the patch antenna element to the reconfigurable pixel surface is 0.525 mm, which is determined by the substrate thickness of the parasitic layer. The substrate for the parasitic layer is also chosen to be quartz. The interconnecting switches used in the simulations are DC contact type MEMS switch [47] of which schematic is given in the inset of Fig. 2.1. A circular metallic membrane made out of gold (Au) is suspended over an actuation electrode to which the DC control voltage is applied. The applied DC voltage creates an electrostatic force between the membrane and the bias electrode. When this force becomes larger than the mechanical force due to the stress of the Au membrane, the membrane moves down and makes a DC contact, thereby connecting the pixels. With no voltage applied the pixels are disconnected. The DC control voltages are applied to the switches via highly-resistive bias lines made out of tantalum nitrite (TaN) with a sheet resistance of approximately 10 kΩ/square and a typical absolute resistance of 600 kΩ. The highly resistive property of the TaN bias lines is advantageous in avoiding any deleterious coupling effect of the EM energy on the pixels.

2.2.2 Reactive Loading and Mutual Impedance

The working mechanism of the "MRA parasitic" presented in this dissertation might best be described by using the theory of reactively controlled directive arrays developed by R. Harrington [29]. In this reference, the radiation characteristics of an antenna system such as the "MRA parasitic," which consists of one driven antenna element and a multiple of parasitic elements, are shown to be controlled by impedance loading of the parasitic

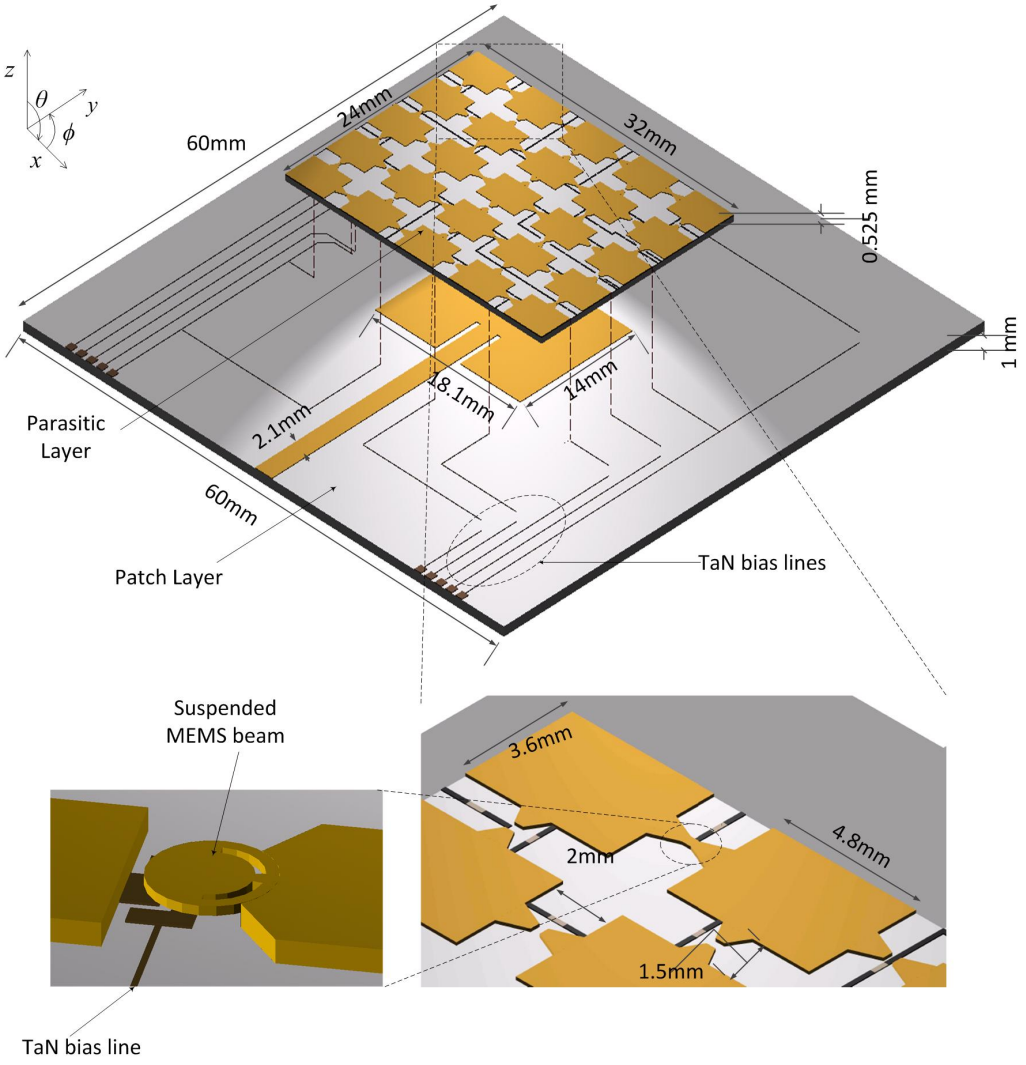

Fig. 2.1: 3D schematic of the MRA parasitic with a magnified view of adjacent pixels and an interconnecting MEMS switch. (For the sake of illustration, the parasitic layer is suspended on top of the patch layer).

elements. The impedance loading occurs due to the EM energy generated by the driven antenna, which couples to the parasitic elements by way of EM mutual coupling. When the parasitic elements are loaded with appropriate reactive loads, the surface current on them can resonate resulting in radiation at a given direction with high gain [20, 29]. In other words, the induced currents on the parasitic elements are maximized when their sizes approach the resonant size. Notice that, for "MRA parasitic" with a given mode of operation, there exist multiple parasitic elements on the reconfigurable parasitic pixel surface. Each parasitic element might consist of a different combination of individual pixels interconnected by switches as shown in Fig. 2.1 (see also Fig. 2.4). As will be shown below, these parasitic elements might possess different surface impedances.

By using circuit theory concepts, the interactions among parasitic elements and the driven element can be described in terms of the mutual impedances with every element being assigned a port [14, 22]. The mutual impedance between the ports of element "i" and element "j" is defined as

$$Z_{ij} = \frac{V_i}{I_j}\Big|_{I_i=0, i\neq j}, \tag{2.1}$$

where V_i is the voltage applied to the port of element "i" and I_j is the current induced on the element "j" when all the ports but jth port is open circuited. When the applied voltages (V_i) are known, the mutual impedances can be calculated independently, thereby the currents in each element can be calculated resulting in the total radiated E-field, which can be given as [29]

$$E_{tot} = \sum_i E(I_i), \tag{2.2}$$

where $E(I_i)$ is the field produced by I_i. Although the interactions taking place in the MRA parasitic is far complex, which renders the derivation of simple analytical expressions difficult, the principles of the previous works [18–20, 29, 48–50, 52–56] equally apply. In the MRA parasitic, the mutual impedances, or equivalently reactive loads, can be varied by changing the shapes and relative locations of the parasitic elements, (by turning on and off the interconnecting switches), which eventually results in the six different modes

of operation corresponding to three beam steering angles ($\theta_i = -30^o, 0^o, 30^o$) and two polarizations ($P_j = Linear, Circular$). The associated total radiated E-fields can simply be expressed as follows

$$E_{tot,m} = \sum_{i,m} E(I_{i,m}), m = 1, 2...6, \tag{2.3}$$

where integer "m" represents each mode of operation.

2.2.3 Surface Waves and Impedances

The reconfigurable radiation characteristics of the MRA parasitic may also be linked to the surface waves existing on the parasitic layer [57]. Surface waves, in general, might be deleterious for standard micro-strip antennas due to the reduction in radiation efficiency and radiation pattern perturbations, which result from the diffraction of surface waves at the edge of the antenna structure in an uncontrolled manner [58, 59]. For example, the rectangular patch shown in Fig. 2.2(a) provides an ideal launch for surface waves, when the substrate thickness t is chosen as follows [52]

$$t > \frac{c}{4f\sqrt{\epsilon_r - 1}}, \tag{2.4}$$

where c is the velocity of light in free space, f is the cutoff frequency for the surface wave mode and ϵ_r is the effective permittivity of the dielectric substrate used. The electric field of a TM polarized surface wave propagating along the metal-dielectric interface of the patch antenna in $+x$ direction with propagation constant k and decay factor α in the $+z$ direction can be expressed as

$$E = E_z e^{j\omega t - jkx - \alpha z}. \tag{2.5}$$

The surface impedance of a flat metal sheet is derived as [60]

$$Z_s = \frac{1 + j}{\sigma\delta}, \tag{2.6}$$

where σ is the conductivity of the metal and δ is the skin depth due to the surface wave

penetration. Hence, the flat metal sheet of good conductivity has low surface impedance allowing the surface waves to propagate a long distance on it. To suppress the surface wave propagation in the patch antenna, thereby improving the performances, high-impedance electromagnetic (HIEM) surface [60] of a periodic structure, such as the one shown in Fig. 2.2(b) [57, 60, 61], can be used. The periodicity in the metallic surface provides high impedance at a specific frequency band, which is used to suppress the surface waves launched by the patch antenna. An HIEM surface is equivalent to a parallel LC resonant circuit, where vertical vias and the gaps between the adjacent metallic pixels provide the necessary inductance and capacitance, respectively. The equivalent surface impedance of a HIEM surface can then simply be expressed as [60]

$$\tilde{Z}_s = \frac{j\omega L}{1 - \omega^2 LC}, \tag{2.7}$$

which becomes very high at resonant frequency,

$$\omega_0 = \frac{1}{\sqrt{LC}}. \tag{2.8}$$

Surface waves have also been utilized to achieve patch antennas with monopole-like radiation pattern with higher gain and low cross polarization [57, 62]. This is an advantage over a standard monopole, as a patch antenna has a lower profile. A patch antenna is loaded with periodic conducting pixels, which is similar to our reconfigurable pixel surface as shown in Fig. 2.3 [62]. The geometry of the pixel surface is, however, fixed by the initial design and cannot be changed. This pixel surface properly controls the propagation of the surface waves, which eventually diffract from the edges of the antenna structure yielding monopole like radiation pattern.

The distinguishing feature of the MRA parasitic presented in this dissertation is the capability of reconfiguring the geometry of the parasitic pixel surface (see Fig. 2.3) by means of switching, which yields multiple parasitic elements as indicated above and shown in Fig. 2.4. The surface impedance of these parasitic elements will vary depending on their

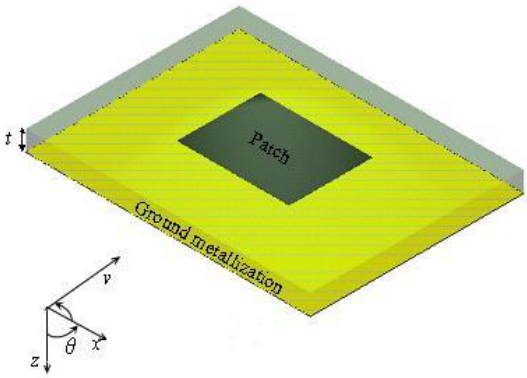

(a)

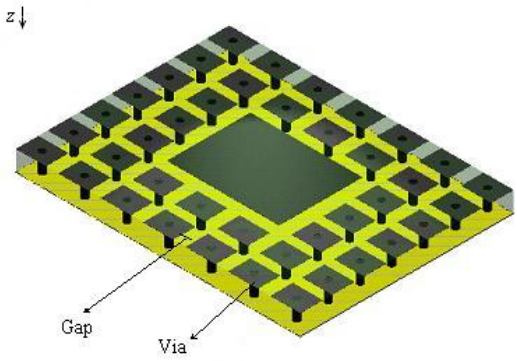

(b)

Fig. 2.2: Schematic showing a transition from a structure supporting surface waves to a HIEM surface suppressing surface waves. (a) Rectangular patch antenna, and (b) HIEM embedded within a patch antenna structure.

shapes and locations with respect to the driven patch antenna. Therefore, while the surface waves will propagate over some parasitic elements they will be suppressed by others. Notice that in our parasitic layer the equivalent inductances and capacitances are due mainly to the metallic strips of the interconnecting switches and the gaps between adjacent pixels, respectively, as shown in Fig. 2.3. In short, our parasitic layer acts as a reconfigurable HIEM surface of which surface impedances over various regions can be changed. This situation is shown in Fig. 2.4, where the reconfigurable pixel surface corresponding to one of the beam steering modes ($\theta = -30^0, P = Linear$) is depicted. As seen from Fig. 2.4, there exist different surface impedances over different regions, i.e., different parasitic elements. According to (2.7), surface waves are supported by regions with low surface impedance, which are not in resonance, and they are suppressed by high impedance regions, which are in resonance. The resulting return loss and radiation pattern obtained by using full-wave analyses software HFSS [46] are given in Fig. 2.5(a) and Fig. 2.5(b), respectively. It is worth noting that with this reconfiguration mechanism, we do not only achieve beam steering but also gain improvement by 1 dB as compared to legacy patch antenna (from 7 dB to 8 dB). It must also be emphasized that the interaction among the parasitic elements with different surface impedances is another factor that plays a role in determining the appropriate reactive loading, which eventually results in the desired mode of operation. Consequently, changing the status of any switch in the low impedance area, where the surface wave is strong, affects the reactive loading of different parasitic elements dramatically; this results in a significant change in radiation properties. For example, changing the status of S1 (see Fig. 2.4) from its original ON to OFF, the input impedance changes significantly as shown in Fig. 2.6. The change in the corresponding radiation pattern is also significant. On the other hand, the pixel elements indicated as P1 and P2 in Fig. 2.4, where the surface impedance is high, play almost no impact on the reactive loading. This is clearly seen in Fig. 2.7(a) and 2.7(b), where the reflection coefficients and radiation patterns for both cases remain almost identical. As shown in Fig. 2.4, the surface geometry of the parasitic layer possesses high degree of reconfigurability due to a large number of metallic pixels (5×5) and

interconnecting switches. Therefore, one can obtain a large number of parasitic elements with various shapes and locations enabling different reconfigurable modes of operation. In other words, the appropriate reactive loads generating the desired modes of operation can be obtained. As will be shown in the next section, the MRA parasitic structure can easily achieve the targeted modes of operations in beam-tilt and polarization by making use of an efficient genetic algorithm in combination with full-wave analyses.

Also, given the symmetric feature of the parasitic layer, once the mode with tilt angle θ has been found, the other mode of $-\theta$ can simply be found by mirroring the switch status along the symmetry axis shown in Fig. 2.3.

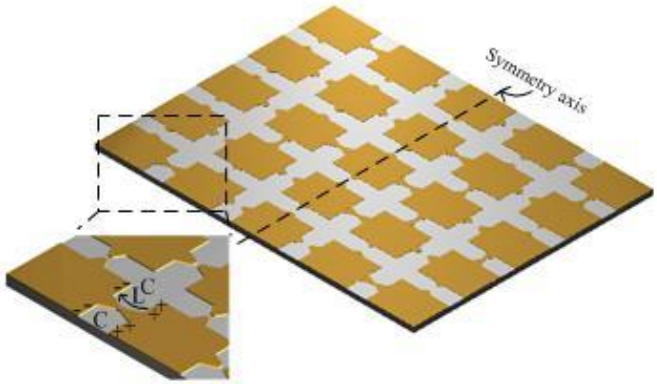

Fig. 2.3: The capacitive and inductive effects occurring at the interconnection area of two adjacent pixels on reconfigurable parasitic pixel surface.

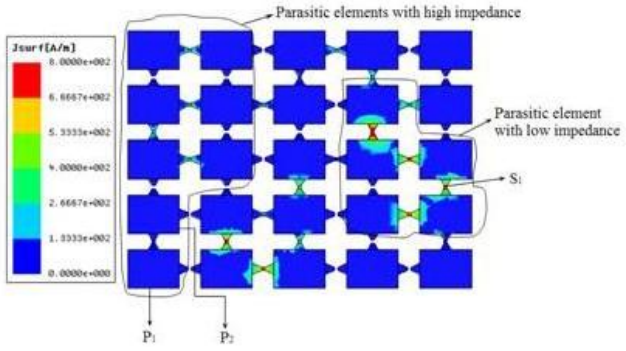

Fig. 2.4: Regions of different surface impedances (parasitic elements) on the reconfigurable pixel surface of the parasitic layer.

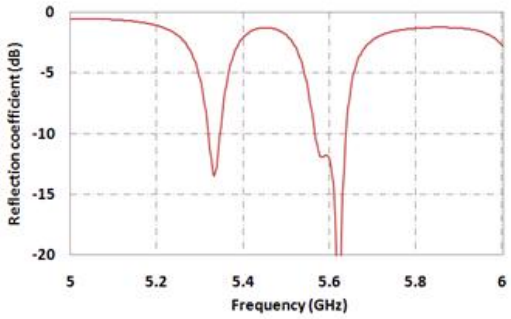

(a) Reflection Coefficient

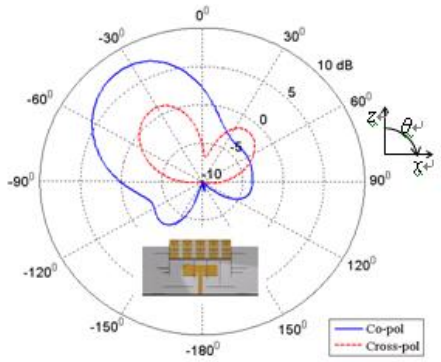

(b) Radiation Pattern (realized gains) at 5.62 Ghz

Fig. 2.5: (a) Reflection coefficient, and (b) radiation pattern (realized gains) at 5.62 GHz of the "MRA parasitic" utilizing the switch configuration in Fig. 2.4.

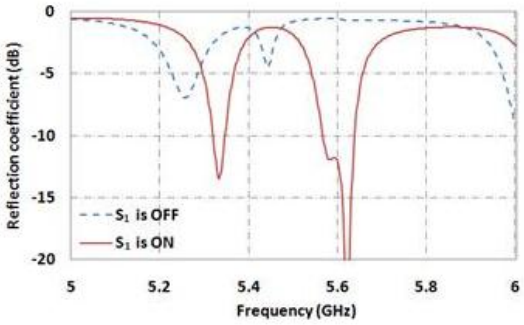

Fig. 2.6: Reflection coefficients of configurations with S1 ON and OFF.

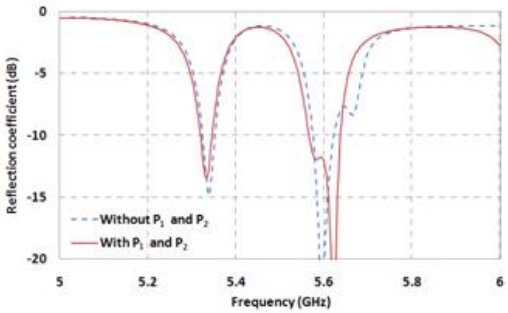

(a)

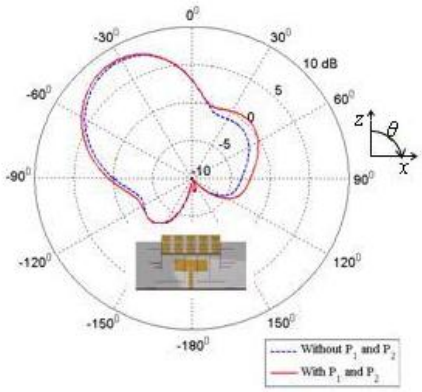

(b)

Fig. 2.7: (a) Reflection coefficients, and (b) radiation patterns (realized gains) of configurations with and without P1 and P2 at 5.62 GHz.

Chapter 3

Design and Optimization Methodology

In this chapter, it is first to provide general description of multi-objective genetic algorithm (GA), before applying it to the specific problem, which is to obtain multiple aims: (a) required realized gain in three directions of arrival, ($\theta_i = -30^o, 0^o, 30^o$), (b) desired bandwidth (BW) of $\sim \%3$ and c) targeted polarization types ($P_j = Linear, Circular$).

In a multi-objective optimization problem, the aim is to find the optimal solution vector of decision variables ($\mathbf{X} = [x_1^*, x_2^*, ...x_d^*]$). This solution vector must satisfy specific constraints such as the ones given in (3.1), in order to produce optimal values for all objective functions $obf_i(x), i = 1, 2, ...m$, which may mathematically be expressed as follows:

$$\begin{aligned} &Minimize(Maximize)\ obf_i(x), && i = 1, 2...m \\ Subject\ to \quad &g_i(x) \leqslant 0\ (g_j(x) \geqslant 0), && j = 1, 2...n \\ &h_k(x) = 0, && k = 1, 2...z \\ &l \leqslant x \leqslant u, \end{aligned} \tag{3.1}$$

where $obf_i(x)$ are objective functions to be optimized, $g_j(x)$ and $h_k(x)$ are inequality and equality constraint functions, and l, u vectors represent lower and upper bounds, respectively.

The multi-objective GA is different from single-objective GA in the sense that, it has more than one aim which conflict each other and should be evaluated simultaneously. Multi-objective optimization problems usually lead to a set of non-dominated solutions, known as Pareto optimal solutions, where each objective corresponding to any point along the Pareto optimal front can only be improved by degradation of at least one of the other objectives [63]. An important concept in multi-objective optimization is that of domination, where a solution x_i is said to dominate another solution x_j if both the following conditions

are true: (a) the solution x_i is not worse than x_j in all objectives, (b) the solution x_i is strictly better than x_j in at least one objective.

Multi-objective GA has been widely used in the last decade to solve electromagnetic engineering problems such as parameter optimizations of different types of antenna designs [35, 36], antenna array optimization [10, 37–40], filter [41], and microwave absorber designs [42–45]. Many different algorithms have thus far been proposed in solving multi-objective problems. Non-dominated sorting genetic algorithm (NSGA) has been one of the most popular, which has an efficient sorting algorithm and incorporates elitism [63]. An improved version of this algorithm is NSGA-II [64], which is used in this work. The working mechanism of NSGA-II is depicted in Fig. 3.1. It starts with a set of solution parameters named as population to be optimized. These parameters are represented by a chromosome, whereby each parameter is encoded in a binary string or real value called gene. In the absence of any clue about the solution, initial population (P_t) is created randomly by using uniform distribution with size N.

All chromosomes in this population are sorted into different front levels based on the domination of pair comparison. Each front level is assigned a fitness (or a rank), which equals its non-domination level. Level 1 is the top level in which the individual is dominated by none of the other individuals; level 2 is the secondary level in which the individual is dominated by some individuals only in level 1, and so on.

In the same front level, the location of the finite number of solutions is expected to be distributed uniformly. In other words, a large diversity of the individuals can prevent the results from trapping into a local optimum. Therefore, another feature, called crowding distance, is adopted to evaluate the local "aggregation" of individuals [64]. The crowding distance is a measure of how close an individual is to its neighbors. Large average crowding distance will result in better diversity in the population. When calculating crowding distance value, as a first step, individuals on the front are sorted for every m^{th} objective by $\mathbf{Sort}(fi; m)$ function, where f_i represents the set of individuals on the i^{th} front. Then, boundary individuals at each pareto front (F_i) are assigned infinite value such as $d_1 = \infty$

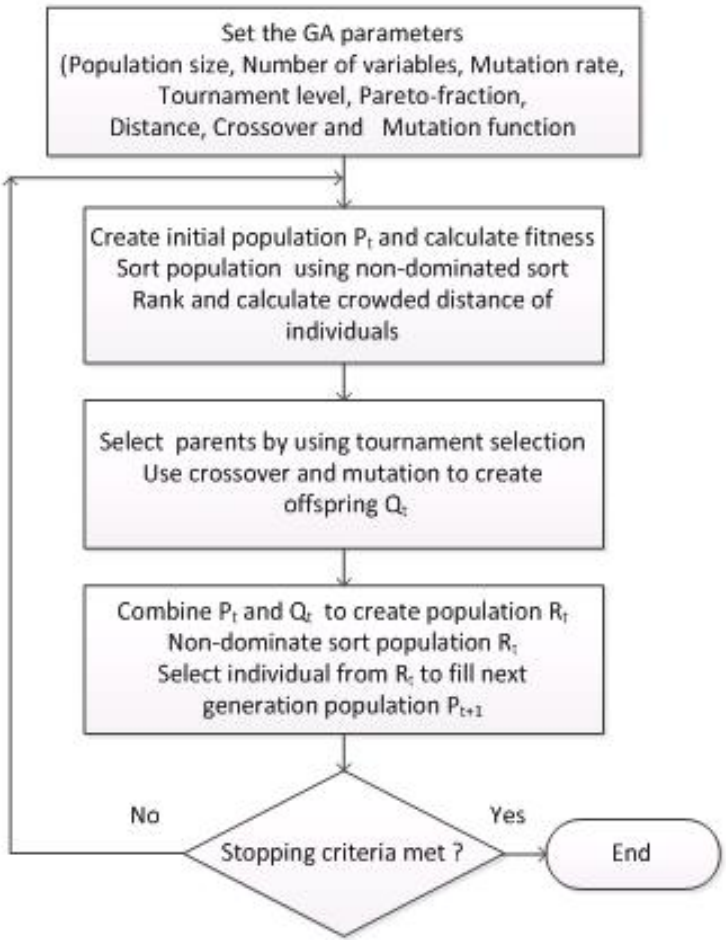

Fig. 3.1: NSGA-II algorithm flow chart.

and $d_n = \infty$ where d_i is the crowding distance value of i^{th} individual, and n is the number of individuals at pareto front F_i. The crowding distance value is calculated as follows:

$$d_k = \sum_{k=2}^{n-1} \sum_{m=1}^{N_{obj}} \frac{obf_{k+1}^m - obf_{k-1}^m}{obf_m^{max} - obf_m^{min}}, \tag{3.2}$$

where obf_k^m is the fitness value of m^{th} objective of k^{th} individual at pareto front F_i, and N_{obj} is the number of objectives.

After each pareto front is ranked and crowded distance is calculated, binary tournament selection is used to select parents to produce offspring. An individual from a pareto front with a higher rank value is selected for reproduction. If the rank values of individuals are the same, then the individual with bigger crowding distance is selected. The selected population generates offspring (Q_t) by using crossover and mutation operators with a user-definable mutation probability (pm). The current generation population (Pt) is combined with the offspring population (Q_t) to produce temporary population (R_t). Since all the previous and current best individuals are added in the population, elitism is guaranteed. After combining process, new temporary population is sorted based on non-domination. The population of next generation (P_{t+1}) is filled by individuals at each pareto front of R_t in a subsequent manner, until the population size exceeds the current population size.

The algorithm execution terminates when the number of generations exceeds a pre-defined maximum number, the fitness value falls below the anticipated threshold, or there is no improvement in solution in the successive iterations. NSGA-II converges to a best pareto-optimal front of non-dominated solutions at the end of algorithm.

Matlab genetic algorithm direct toolbox [65] and full wave analysis software HFSS [46] are jointly used to solve our optimization problem. A schematic is shown in Fig. 3.2. Interface between the Matlab and HFSS is implemented through the Matlab-API (application program interface) files. Matlab GA creates script file for a given configuration, which is coded in chromosomes. HFSS loads this file and runs a full-wave simulation to create the report needed by GA to calculate fitness values.

Our optimization problem is combinatorial optimization, whose parameters are the

states of interconnecting switches (on = "1", off = "0"), placed between adjacent metallic pixels of the reconfigurable parasitic pixel surface. This surface consists of a grid of 5×5 pixels as shown in Fig. 2.1, with 40 switches, where there are 2^{40} possible switch status permutations to be tested in search space. The overall optimization process can be explained as follows:

(1) The optimization process starts with coding the design parameters. The binary and real value representation of the chromosome structure of the reconfigurable parasitic pixel surface are shown in Fig. 3.3. Real coded genetic algorithm is used in our application. Each chromosome vector has nine genes, which are bounded real values, in order to avoid the values to be out of range when mutation and crossover operations are performed. The first five genes (bounded between 0 and 15) represent each row of horizontally oriented switches, where each row has four switches (= 4 bits) as shown in Fig. 3.3. Similarly, the rest of the four genes (bounded between 0 and 31) correspond to the vertically oriented switches, where each row has five switches (=5 bits).

(2) In the second step, multi-objective functions are determined allowing the evaluation of the solutions, which are the desired switch configurations yielding our aims: (a) required

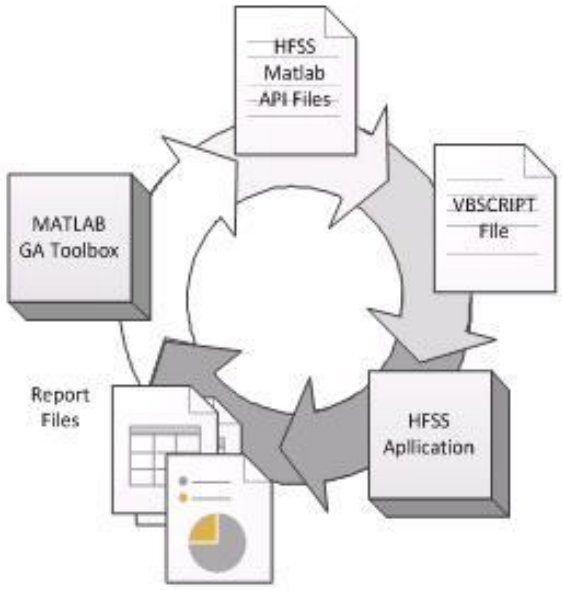

Fig. 3.2: The schematic of the Matlab GA toolbox-HFSS interface.

tilt gain in three directions of arrival ($\theta_i = -30^o, 0^o, 30^o$), (b) desired frequency bandwidth (BW) of $\sim$ % 3, and (c) targeted polarization types ($P_j = Linear, Circular$). The objective functions along with associated graphs are given below:

$$\begin{aligned} obj_1 &= obf_{Gain\_dB}(f_0, \theta_{DOA}, \phi_{DOA}) \\ obj_2 &= obf_{BW}(|S_{11}|, -10dB) \\ obj_3 &= obf_{pol}(AR, f_0, \theta_{DOA}, \phi_{DOA}), \end{aligned} \tag{3.3}$$

where f_0 is the expected frequency, θ_{DOA} and phi_{DOA} describe the tilt direction as defined in Fig. 3.4(a), AR is the axial ratio for polarization, and $|S_{11}|$ represents the magnitude of reflection coefficient. The function obf_{Gain_dB} yields maximum realized gain at the given frequency and direction of arrival. Notice that obj_1 is the realized gain which takes into account the losses due to input impedance mismatch. obf_{BW} function gives the range of frequencies for which $|S_{11}|$ satisfies VSWR $\leqslant 2$ as shown in Fig. 3.4(b). Using a range of frequencies as opposed to the minimum reflection coefficient at a single frequency value avoids any misleading effect on fitness, because, generally, patch antennas have narrow bandwidths with low $|S_{11}|$. On similar lines, instead of using a single AR value in determining the status of polarization in objective function 3, this value is fuzzified by using obf_{Pol} fuzzy membership function as given in (3.3). Output of this function, which is between 0 and 1, shows how linearly or circularly polarized the EM wave is, as shown in Fig. 3.4(c). For circu-

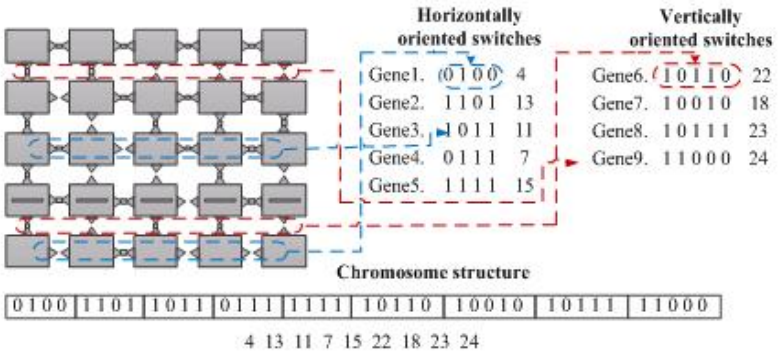

Fig. 3.3: Chromosome coding optimization process for reconfigurable parasitic pixel surface of 5×5 pixels.

lar polarization, obf_{Pol} function is given in (3.3), whereas for the linear polarization, the complement of equation (3.3) is used.

Corresponding to three directions of arrival ($\theta_i = -30^o, 0^o, 30^o$) and two polarization types ($P_j = Linear, Circular$), six optimization problems are defined. These optimization problems are solved with GA parameters listed in Table 3.1. Each problem has a Pareto optimal surface which contains more than one solutions satisfying the three aims, namely, required realized gain in a given direction of arrival, ($\theta_i = -30^o, 0^o, 30^o$), desired BW of $\sim \%3$, and targeted polarization types ($P_j = Linear, Circular$). To select the best designs for implementation among these Pareto-optimal surfaces, we take into account the common frequency BW in conjunction with realized maximum gain. Finally, in selecting the best designs, an expert eye is used. The corresponding switch configurations and the results are discussed in the next chapter.

$$obf_{pol} = \begin{cases} 0 & \text{AR} \leqslant 3dB \\ -\frac{1}{7}(AR - 10) & \text{3dB} \leqslant \text{AR} \leqslant \text{10dB} \\ 1 & \text{AR} \geqslant \text{10dB} \end{cases} \tag{3.4}$$

Table 3.1: NSGA-II running parameters.

Parameters	Value
Number of variables(chromosome length)	9
Population	40
Generatin	30
Mutation rate	0.1
Tournament level	2
Distance function	Crowding distance(eqn 3.2)

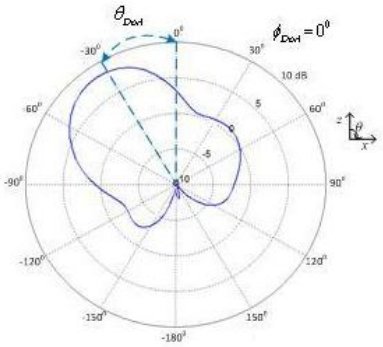

(a) $obf_{Gain\_dB}(f_0, \theta_{DOA}, \phi_{DOA})$

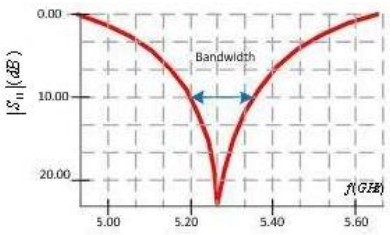

(b) $obf_{BW}(|S_{11}|, -10dB)$

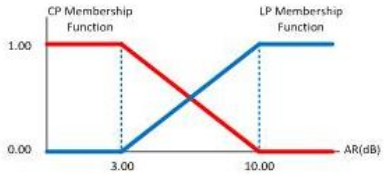

(c) $obf_{pol}(AR, f_0, \theta_{DOA}, \phi_{DOA})$

Fig. 3.4: Schematics showing objectives of optimization problem: (a) objective 1, (b) objective 2, and (c) objective 3.

Chapter 4

Results and Discussions

4.1 Simulated Results for MRA Parasitic

The geometries of the reconfigurable parasitic pixel surface of the parasitic layer corresponding to each of the six modes of operations (three different beam directions and two polarizations) are shown in Fig. 4.1. The simulations with and without DC bias-lines have been shown to yield almost identical results. This is due to the highly-resistive property of the TaN bias lines. Therefore, for simplicity, in avoiding simulations with exceedingly large size, the bias lines are omitted in the simulations. While in the simulations the exact geometry of the MEMS switches are used, for the sake of illustration the off-state switches are represented by perfect open circuits and the on-state switches are shown as perfect short circuits in Fig. 4.1. As described in the previous section the optimized configurations of the interconnecting switches have been determined by multi-objective GA in conjunction with full-wave analyses. Notice that in Fig. 4.1, the pixels in the fourth row have rectangular slits. These slits are useful in obtaining circular polarizations, where two orthogonal E-field components with 90^o phase difference between them can be excited.

From the reflection coefficients shown in Fig. 4.2, the center frequency for all of the modes of operation is around 5.25 GHz with a common frequency bandwidth of 1%. The realized gain patterns at 5.25GHz in three different directions: $(\theta_i = -30^o, 0^o, 30^o)$ with linear and circular polarizations are shown in Fig. 4.3(a) and 4.3(b), respectively. The maximum realized gain values for all the modes of operation are around 8 dB. Table 4.1 gives the axial ratio values, which confirms that reasonably well linear and circular polarizations have been obtained for all modes of operations.

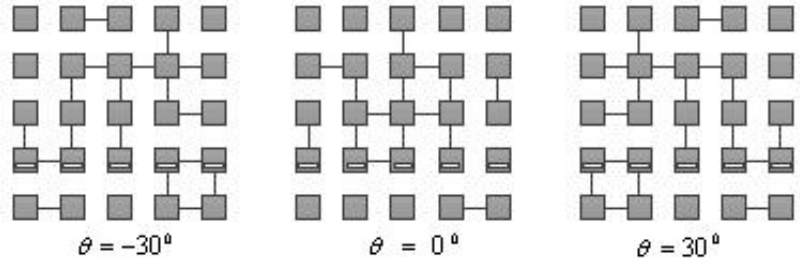

(a) Circular Polarization

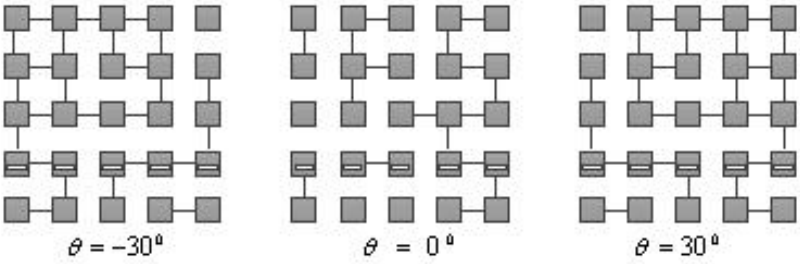

(b) Linear Polarization

Fig. 4.1: Optimized switch configurations for six different modes of operation: (a) circular polarization, and (b) linear polarization.

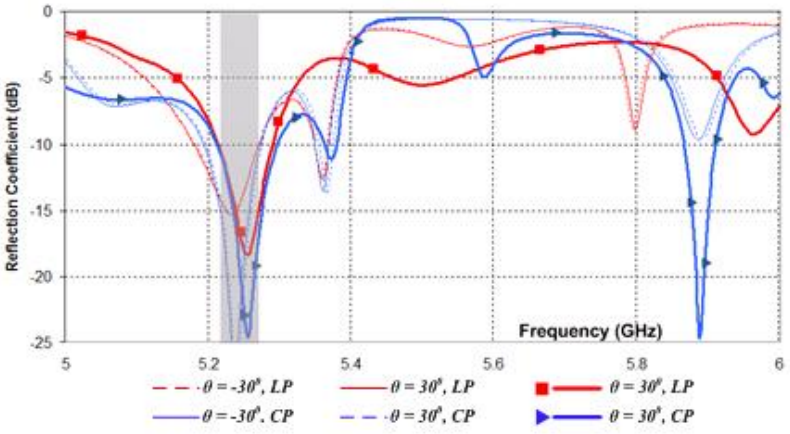

Fig. 4.2: Reflection coefficients of six modes of operation with a 1% common bandwidth highlighted.

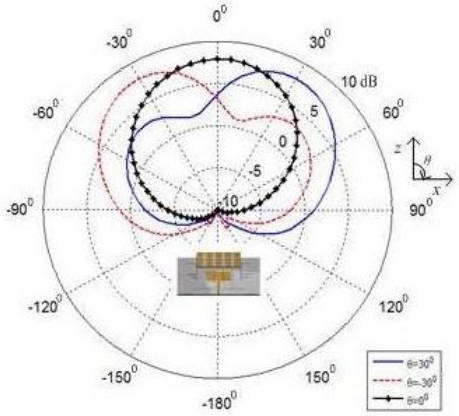

(a)

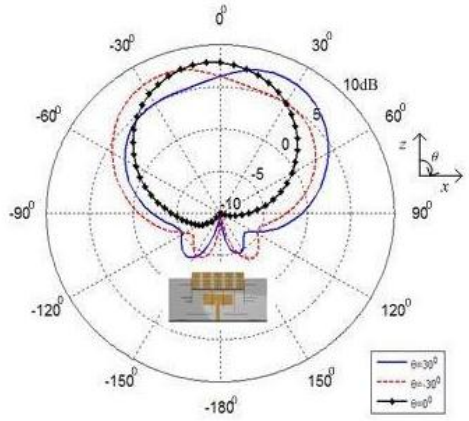

(b)

Fig. 4.3: Realized gain patterns in the x-z plane for three different directions ($\theta_i = -30^o, 0^o, 30^o$) at 5.25 GHz: (a) linear polarization, and (b) circular polarization.

Table 4.1: Axial ratios for different beam directions at 5.25 GHz.

Axial Ratio (dB)	-30^o	0^o	30^o
LP	27.5	18.5	26.8
CP	1.7	5.1	1.7

4.1.1 Prototype

To validate the theoretical analyses along with simulated results of the MRA parasitic presented thus far, three prototypes each of which corresponding to one of the beam steering angle ($\theta_i = -30^o, 0^o, 30^o$) with linear polarization have been designed and fabricated. The radiation and impedance characteristics of these prototypes have been measured and compared with those of the simulated results. Vector network analyzer (VNA) and spectrum analyzer are used in measurement as explained in Appendix B.

The parasitic and the driven patch antenna layers were fabricated separately, which were then bonded together to obtain the prototypes. Gold (Au) metal (conductivity: $\sigma = 4.098 \times 10^7 S/m$) is deposited on quartz substrates by an electron beam deposition tool and chemically etched in a clean room environment to form the patch antennas and the pixels of the parasitic layer. The thicknesses of the quartz substrates of patch and parasitic layers are 1.00 and 0.525 mm, respectively.

The MRA parasitic prototypes were designed to operate at around 5.6GHz. Figure 4.4(a) and 4.4(b) show the measured and simulated reflection coefficients corresponding to beam-steering ($\theta = 30^o$) and patch ($\theta = 30^o$) modes. Notice that the reflection coefficient is only shown for one of the two beam-steering modes as they have identical results due to the symmetry feature as explained above. As is seen from these figures, although the simulated and measured results agree reasonably well, there is some discrepancy for the beam-steering mode. This can mainly be attributed to the inaccuracies of the fabrication and alignment between patch and parasitic layers.

The radiation patterns of beam-steering and patch modes, shown in Fig. 4.5(a) and 4.5(b), respectively, are with good agreement between simulated and measured results. The patterns are cut in the x-z plane at the center frequencies shown in Fig. 4.4. It is observed that the realized gain values are above 8 dB for all modes.

4.1.2 Conclusions

A parasitic layer based multi-functional reconfigurable antenna (MRA), which can achieve six different modes of operation corresponding to three beam directions ($\theta_i =$

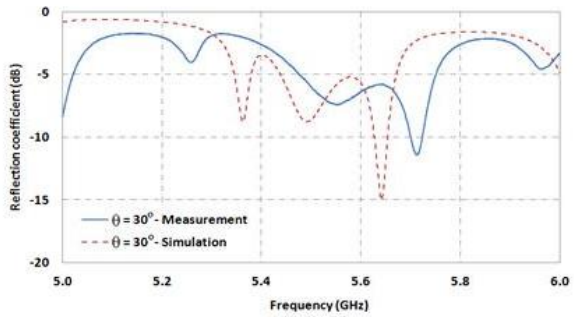

(a)

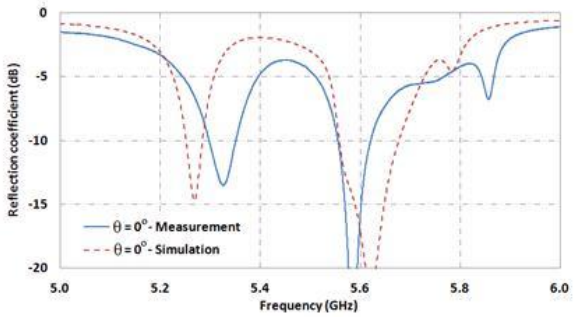

(b)

Fig. 4.4: Measured and simulated reflection coefficients of the MRA parasitic prototypes for beam steering angles (a) $\theta = 30^o$ and (b) $\theta = 0^o$.

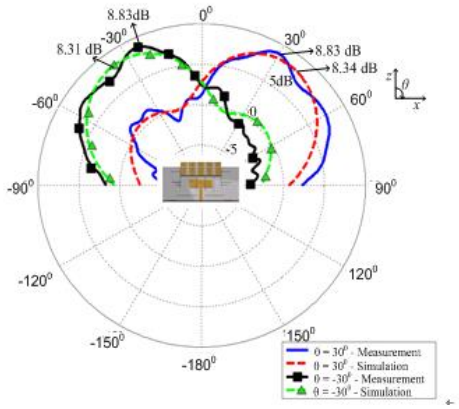

(a)

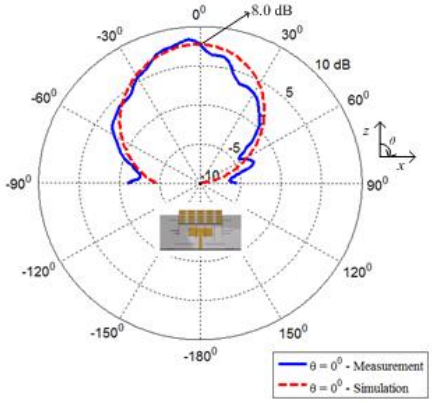

(b)

Fig. 4.5: Measured and simulated realized gain patterns of the MRA parasitic prototypes for (a) beam-steering modes, and (b) patch modes.

$-30^o, 0^o, 30^o$) and two polarizations ($P_j = Linear, Circular$), was introduced in this dissertation. The MRA architecture provides significant advantages both in terms of design and manufacturing as the driven antenna and the reconfigurable parasitic layers are separated from each other. Given the large number of modes of operation, an efficient design methodology which combines multi-objective genetic algorithm and full-wave analyses was employed. We also provided a basic theoretical framework based on the concepts of reactive loading and surface waves describing the working mechanism of the antenna. Prototype antennas were designed, fabricated, and measured which confirmed the accuracy of the theoretical results. The results from measurements and simulations agreed well indicating that the MRA presented can achieve 8 dB gain for all modes of operations. Our ongoing work involves the MEMS fabrication of the MRA parasitic, for which the design and initial fabrication efforts of this work is providing valuable guidance.

Chapter 5

X Band Beam Steering Patch Antennas

5.1 Introduction

The X band is a segment of the microwave radio region of the electromagnetic (EM) spectrum. In some cases, such as communication engineering, the frequency range of X band is rather indefinitely set at approximately 7.0 to 11.2 gigahertz (GHz). In radar engineering, the frequency range is specified by the IEEE at 8.0 to 12.0 GHz.

Some X band applications include satellite communications systems for weather monitoring. Portions of the X band are assigned by International Telecommunications Union (ITU) exclusively for deep space telecommunications. The primary user of the allocation is the American NASA Deep Space Network (DSN). The Radio Regulations of the ITU allow amateur radio operations in the frequency range 10.000 to 10.500 GHz, and amateur satellite operations are allowed in the range 10.450 to 10.500 GHz. Motion detectors often use 10.525 GHz to 10.4 GHz for traffic light crossing. Many electron paramagnetic resonance (EPR) spectrometers operate near 9.8 GHz.

5.2 Inset Micro-Strip Feed Design

5.2.1 Structure

A beam steering patch antenna design operating within X band is introduced in this chapter. In this design, micro-strip fed basic patch is shown in Fig. 5.1, and the whole design in which both basic patch and parasitic layer are included is shown in Fig. 5.2. The structure of this X band MRA is very similar with that of the WLAN MRA studied in the previous sections. However, the substrate material is chosen to be SU-8 ($\epsilon_r \approx 3, tan\delta = 0.04$) in this X band design. SU-8 has the advantage of being microfabrication compatible over standard

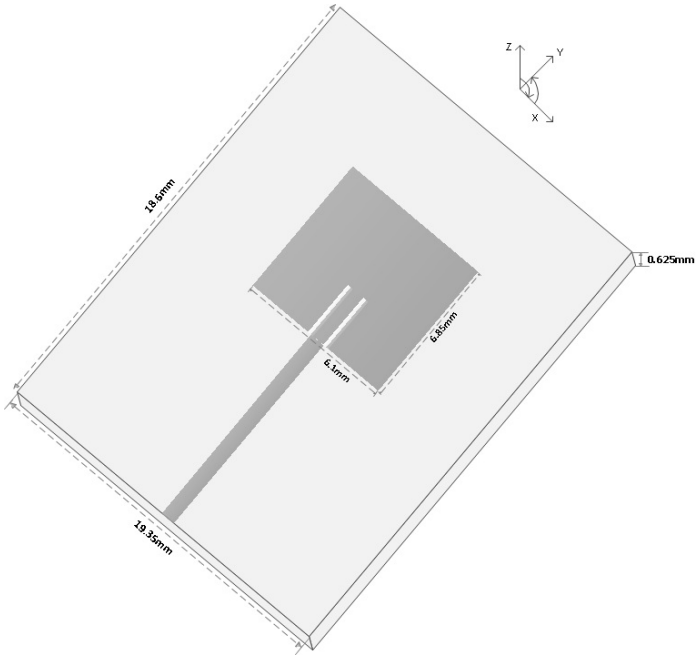

Fig. 5.1: Schematic of the basic micro-strip feed patch antenna of the X band MRA for beam steering.

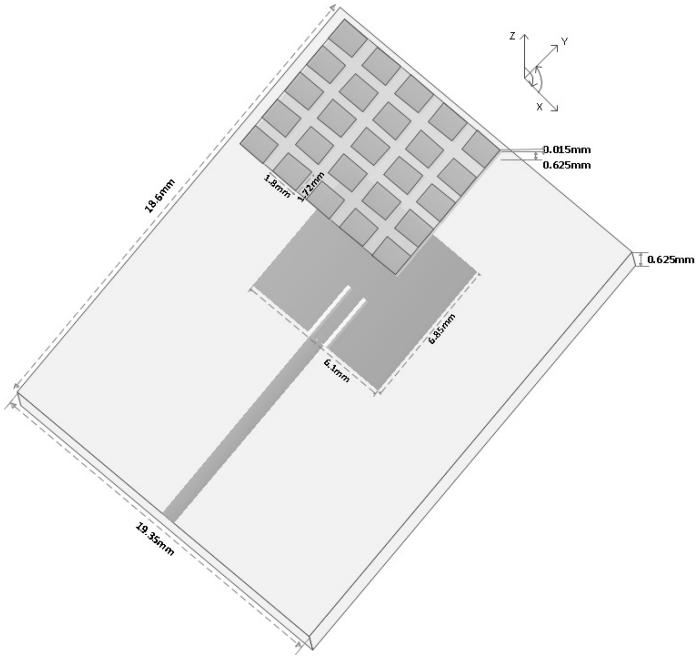

Fig. 5.2: Schematic of overall antenna design.

PCB substrates. Another option is using bisbenzocyclobutene (BCB), Polydimethylsiloxane (PDMS), which has some challenges in microfabrication processes. The thickness of the substrate for basic patch is 0.625 mm, and the one for parasitic pixel layer is 0.015 mm. Between the basic patch and the parasitic substrate, there is an air layer with the thickness of 0.625 mm. The pixel size is $1.8mm \times 1.72mm$ The resonant frequency of this antenna design is in X band (12 GHz), and its beam could be steered into three different directions ($\theta_i = -15^o, 0^o, 15^o$).

5.2.2 Simulation Results

The working mechanism and optimization methodology of the X band MRA is the same with WLAN MRA, therefore it will not be repeated again in this chapter. From the reflection coefficients shown in Fig. 5.3, the center frequency for all of the modes of operation is around 12 GHz with a common frequency bandwidth of 2%. Figure 5.4(a), Fig. 5.4(b), and Fig. 5.4(c) show the realized gain patterns at 12GHz in three different directions: ($\theta_i = -15^o, 0^o, 15^o$). The maximum realized gain value is 5 dB.

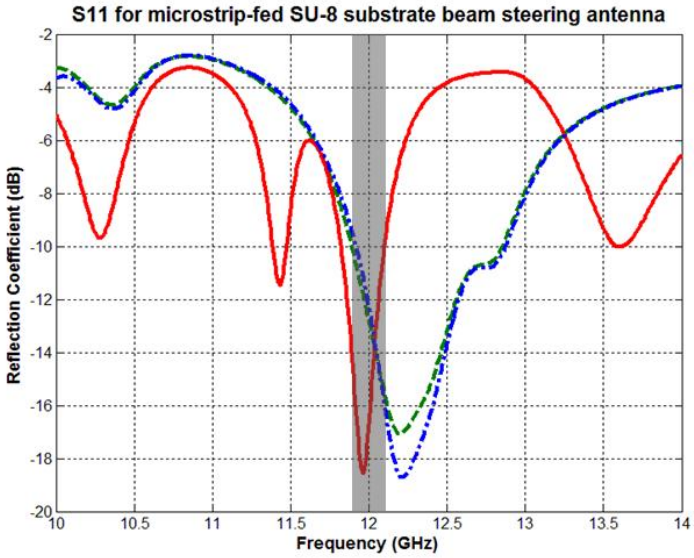

Fig. 5.3: Reflection coefficients of three modes of operation with a 2% common bandwidth highlighted.

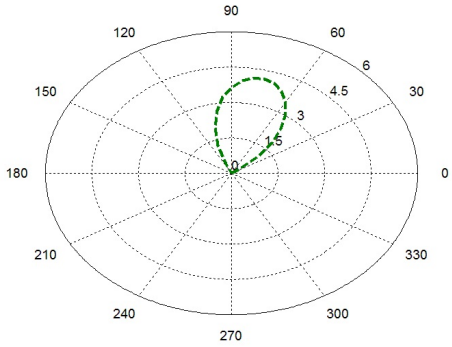

(a) $\theta_i = -15^o$

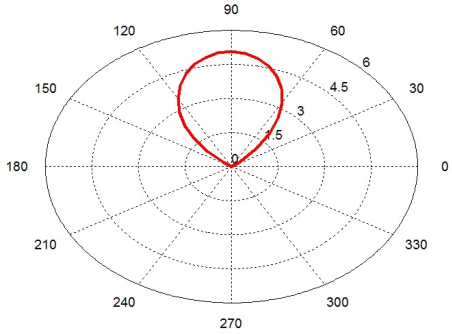

(b) $\theta_i = 0^o$

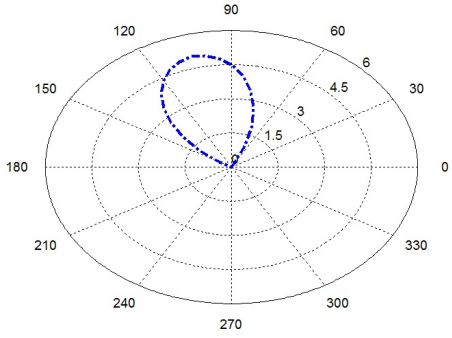

(c) $\theta_i = 15^o$

Fig. 5.4: Realized gain patterns of the micro-strip fed beam steering antenna in the x-z plane for three different directions ($\theta_i = -15^o, 0^o, 15^o$) at 12 GHz.

5.3 Aperture-Coupled Feed Design

5.3.1 Structure

Another beam steering X band patch antenna design is presented here. In this design, we employed an aperture-coupled feed mechanism as opposed to inset feed mechanism as shown in Fig. 5.5. The main advantages of this feed mechanism is to provide wider common frequency bandwidth, better beam steering capability, and higher realized gain on the desired beam direction as compared with inset micro-strip fed. Aperture coupled feeding technique uses two layers of substrate. One layer is for the basic driven antenna element, with the thickness of 1.524mm; and the other layer on the bottom one is for the aperture couple feed, with the thickness of 0.508mm. Both substrates are Rogers RO4003 ($\epsilon_r = 3.55, tan\delta = 0.0027$). The design schematic including parasitic layer is shown in Fig. 5.6. The structure is very similar with the micro-strip fed MRA. The parasitic substrate is also SU-8 with a thickness of $15\mu m$. There is also an air layer between the patch and parasitic substrate, for which the thickness is $2.5mm$. The pixel size is $2.4mm \times 1.8mm$. The resonate frequency of this antenna design is also in X band, and its beam could be steered into three different directions ($\theta_i = -30^o, 0^o, 30^o$).

5.3.2 Simulation Results

From the reflection coefficients shown in Fig. 5.7, the center frequency for all of the modes of operation is around 12 GHz with a common frequency bandwidth of 4%.

Figure 5.8(a), Fig. 5.8(b), and Fig. 5.8(c) show the realized gain patterns at 12GHz in three different directions: ($\theta_i = -30^o, 0^o, 30^o$). The maximum realized gain value is 7.8 dB.

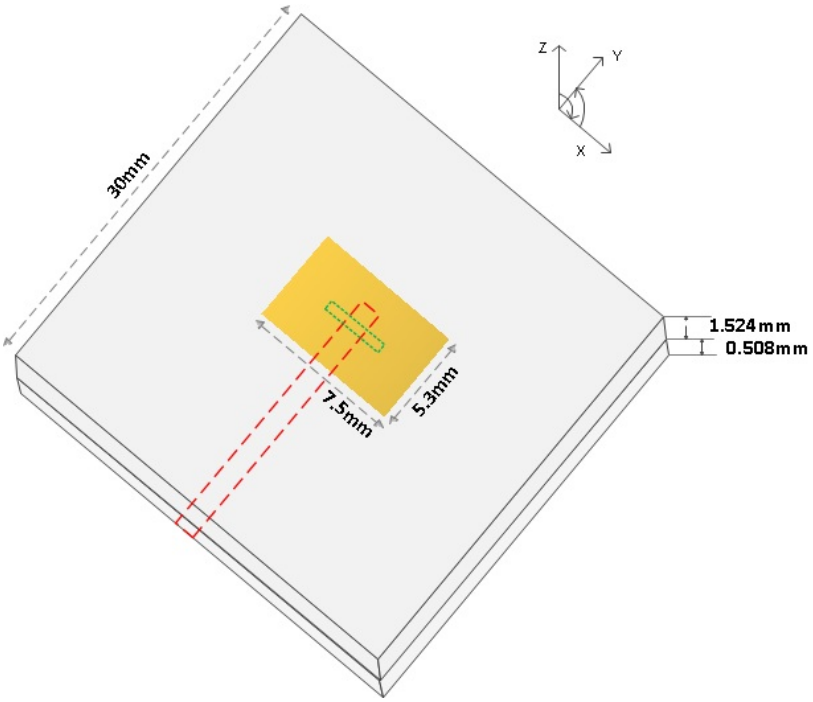

(a)

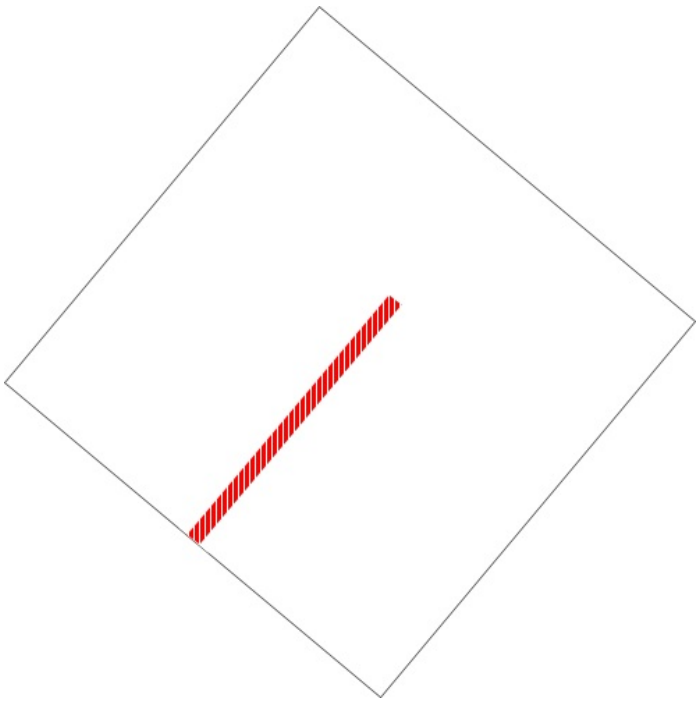

(b)

Fig. 5.5: Schematic of an aperture-coupled inset micro-strip line feed basic driven patch in X band beam steering design: (a) schematic of aperture-coupled inset micro-strip line fed basic driven patch in X band beam steering design, and (b) inset micro-strip line for the feed surface.

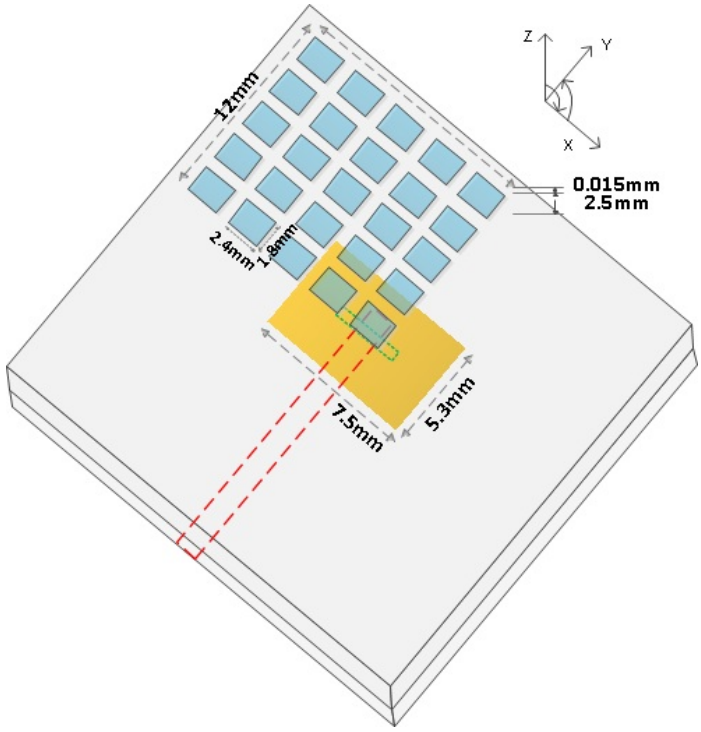

Fig. 5.6: Schematic of beam steering antenna design.

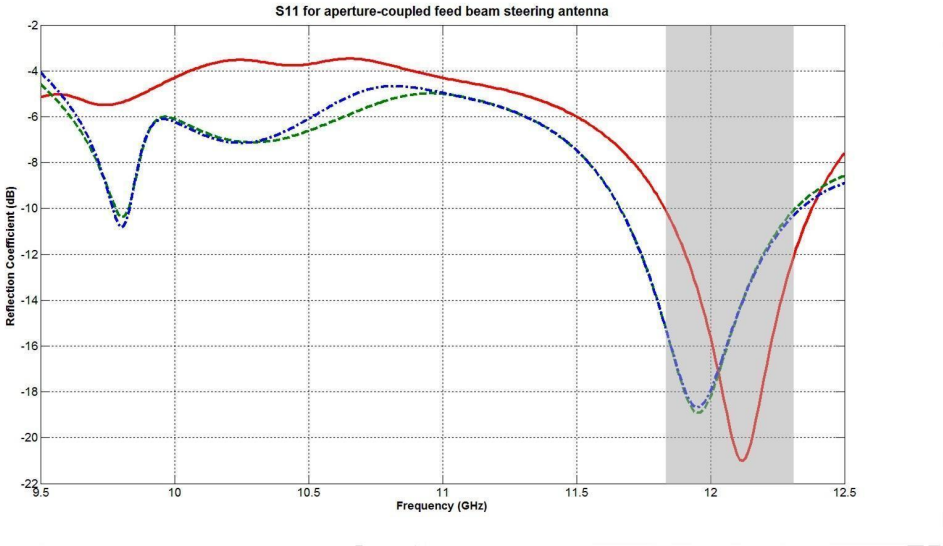

Fig. 5.7: Reflection coefficients of three modes of operation with a 4% common bandwidth highlighted.

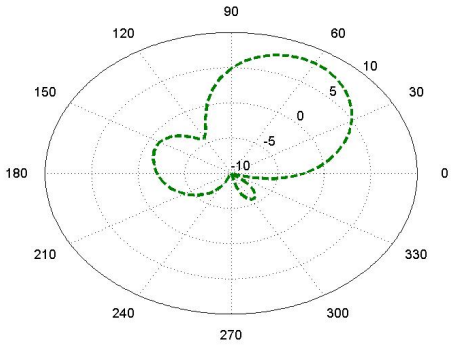

(a) $\theta_i = -30^o$

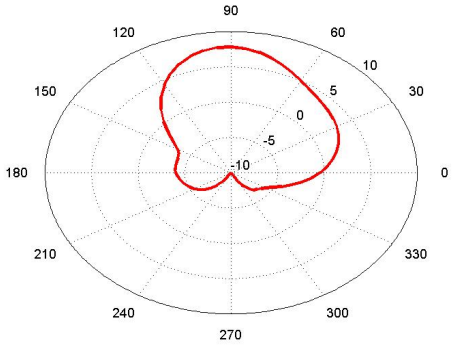

(b) $\theta_i = 0^o$

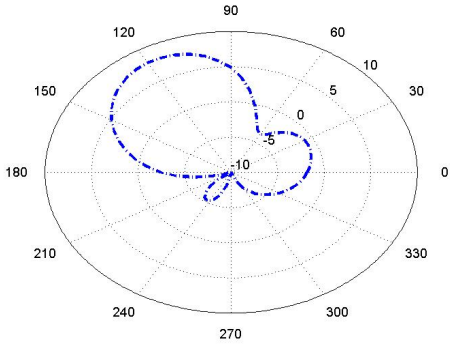

(c) $\theta_i = 30^o$

Fig. 5.8: Realized gain patterns in the x-z plane for three different directions ($\theta_i = -30^o, 0^o, 30^o$) at 12 GHz.

Chapter 6

60 GHz MRAs for WPAN

6.1 Introduction

A personal area network (PAN) is a computer network used for wireless communications among computerized devices, including telephones and personal digital assistants. PANs can be used for communication among the personal devices themselves or for connecting to a higher level network and the Internet. A WPAN is a PAN carried over wireless network technologies such as Infrared Data Association (IrDA), Bluetooth, Wireless USB, Z-Wave, ZigBee, or even Body Area Network. Wireless PAN is based on the standard IEEE 802.15. The three kinds of wireless technologies used for WPAN are Bluetooth, IrDA, and Wi-Fi. IEEE 802.15 standard relates to broadband antennas of compact size which are capable of receiving or transmitting multi-polarized electromagnetic radiation over wide band while maintaining uniform radiation pattern and impedance characteristics within the operating band. Now, the problem of responding to transmitted signals over a broad band for multi-sense of polarizations could be solved by MRAs.

6.2 Dual Frequency/Dual Polarization Antenna for WPAN

Two different types of NEMS integrated MRA designs will be presented in this chapter. One is capable of changing its operating frequency over two bands and the other one is capable of changing the sense of polarization from linear to circular, for IEEE 802.15 wireless personal area network (WPAN) applications.

These MRAs are designed on benzocyclobutene (BCB) polymer with a relative permittivity of 2.6 and thickness of 0.1mm. BCB is chosen due to its high performance RF characteristics and compatibility with micro fabrication processes at the 60GHz frequency bands. The feeding of square patch is performed with coplanar waveguide (CPW) in order

to reduce transmission line losses. Because of the high impedance nature of CPW structures, the antenna is preceded by a quarter-wavelength impedance transformer, which results an input impedance of 50 Ω. Given the nature of the application and the operating frequency, the CPW line has been designed by taking into account the manufacturing limitations and tolerances, together with the dimensions of a standard 150μm pitch ground-signal-ground (GSG) probe, which will be used for the measurements in the future work. The square patch of dual polarization MRA contains a truncated corner, where a metallic segment can be connected/disconnected, thereby providing both circular and linear polarizations. The square patch of dual frequency MRA uses a pair of inserted slits, which provides resonance frequencies that can be tuned over 57 GHz and 64 GHz. Different modes of operations are implemented by nano-electromechanical systems (NEMS) switches strategically located in each slit gap. It is worth noting that while changing the modes of operation, the radiation characteristics (gain, shape of the pattern) are maintained in these designs.

6.2.1 Structures

The initial schematics of dual-polarization/dual-frequency MRAs are shown in Fig. 6.1(a) and 6.1(b), respectively. The MRAs are built on a substrate of BCB polymer ($\epsilon = 2.6, tan\delta == 0.0008$), with a thickness of 100μm.

6.2.2 Simulation Results for Dual Frequency/Dual Polarization Designs

The dual frequency MRA is proven to work well on two sub-frequency spectrums in the Fig. 6.2(a). And in Fig. 6.2(b), although the dual polarization MRA could shift the type of polarization between linear and circular, there is a common frequency bandwidth for two modes of polarizations. The common frequency band of S11 below -10 dB in Fig. 6.2(b) is from 59.3 GHz to 61.3 GHz, which has a bandwidth of 3.33%. The frequency band of circular polarization for 3 dB axial ratio is from 59.6 GHz to 60.2 GHz. For the linear polarization mode, the axial ratio is always above 10 dB over the common frequency band.

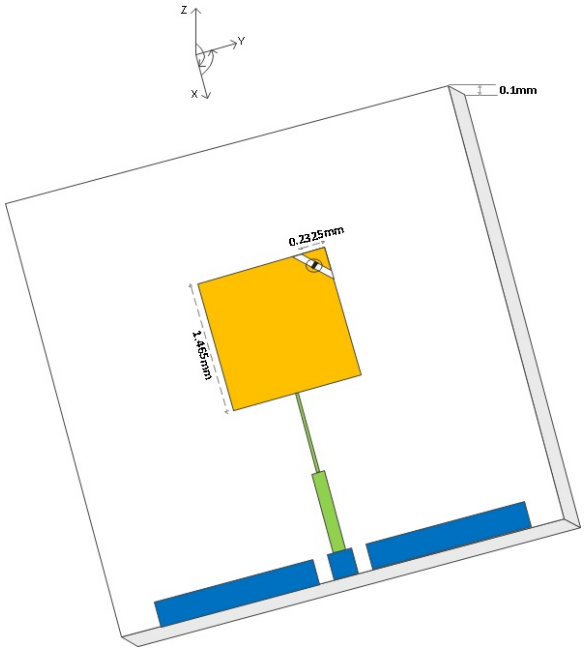

(a)

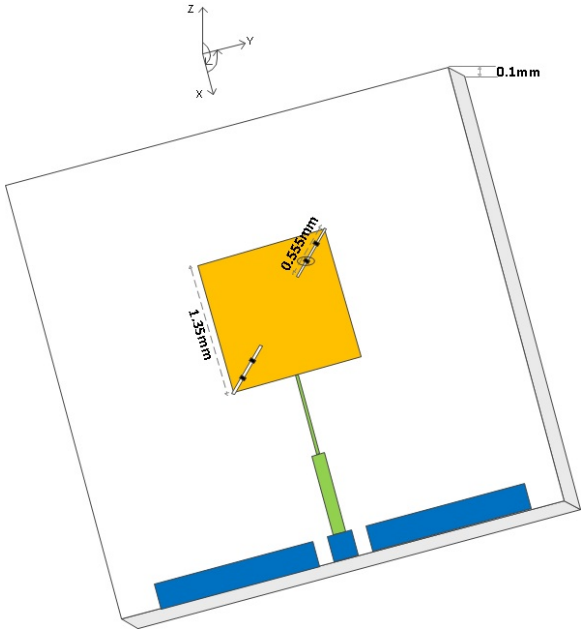

(b)

Fig. 6.1: Structures of dual-polarization/dual-frequency MRAs: (a) dual polarization MRA, and (b) dual frequency MRA.

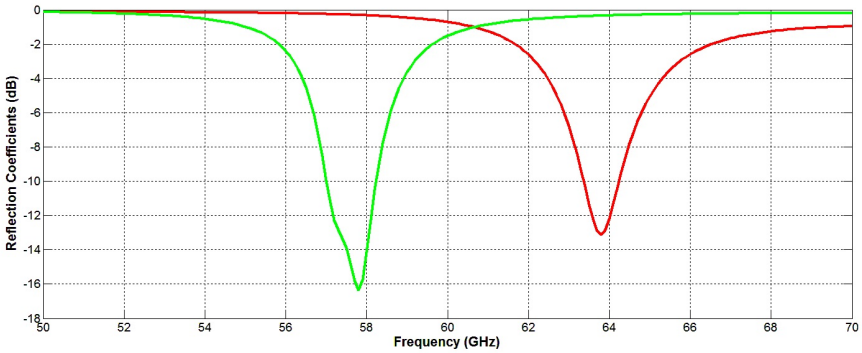

(a)

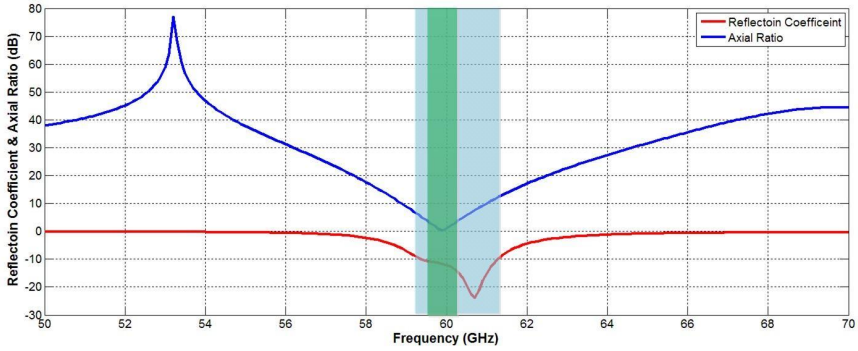

(b)

Fig. 6.2: Simulation results of dual-polarization/dual-frequency MRAs: (a) impedance characteristics for dual frequency MRA, and (b) reflection coefficient and axial ratio value for dual polarization MRA.

6.3 Beam Steering Patch for WPAN

Finally, some initial design efforts on the beam steering antenna operating in the 60GHz bandwidth are presented. This design is shown in Fig. 6.3(a).It is also fed by an aperture-coupled feed mechanism, similar to the previous design as shown in Fig. 5.5(a). The only difference in this design is to use coplanar waveguide as opposed to micro-strip as shown in Fig. 6.3(b).

The initial simulation results are given in Fig. 6.4(a) and Fig. 6.4(b), which show that the driven antenna element resonates at 60 GHz and the shape of radiation pattern is conforming with that of a patch antenna with a maximum realized gain of 3.5 dB.

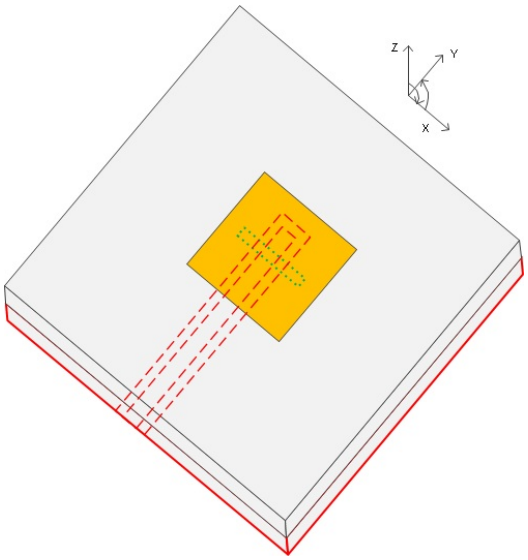

(a)

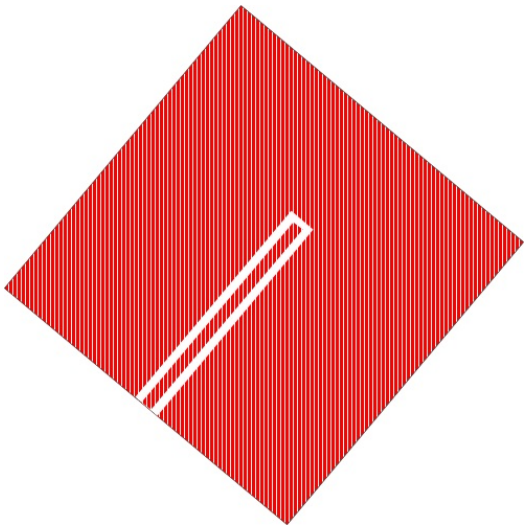

(b)

Fig. 6.3: Schematic of aperture-coupled CPW fed basic driven patch on 60 GHz: (a) schematic of aperture-coupled CPW fed basic driven patch on 60 GHz, and (b) CPW for the feed surface.

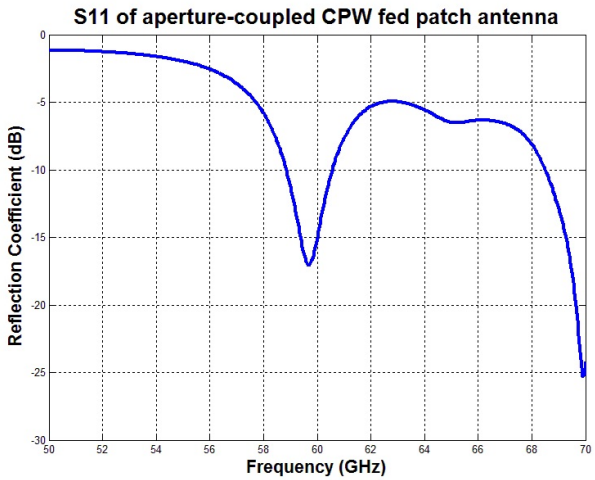

(a)

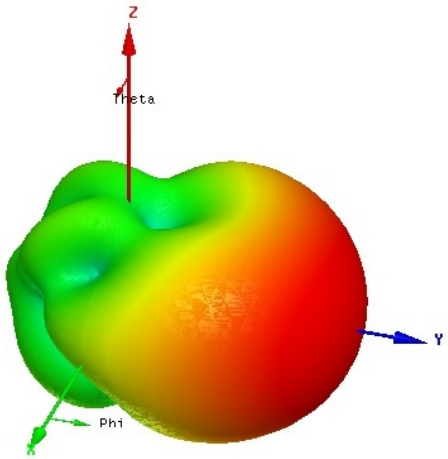

(b)

Fig. 6.4: Simulation results of aperture-coupled CPW fed basic driven patch on 60 GHz: (a) reflection coefficient, and (b) 3D radiation pattern.

Chapter 7

Conclusions and Future Work

Because of the significant performance advantages as compared to multiple single-function antennas, multi-functional reconfigurable antennas (MRAs) have gained substantial interests with the goal of enhancing the performances of today's transmitting and receiving wireless communication systems. This dissertation work concentrated on the development of various types of MRAs. These are parasitic layer-based reconfigurable antenna designs for use in wireless local area network (WLAN) applications, X band beam steering applications, and 60 GHz wireless personal area network (WPAN) dual frequency, dual polarization and beam steering applications.

The design and full-wave analyses of these MRAs have been presented. The parasitic layer-based reconfigurable WLAN patch antenna could provide three beam directions (-30^0, 0^0, 30^0) as well as two types of polarizations (linear and circular) on each direction. Quartz is chosen as the substrate for both driven antenna element and parasitic layer structures. Various prototypes for the WLAN antenna have been fabricated and characterized in order to validate the accuracy of the theoretical methods and the results. The measurement results are proven to match well with the simulation results. The common frequency bandwidth over the expected center resonate frequency 5.25GHz is around 1%, and the maximum realized gain on three steered beam directions are as high as 8 dB. This is approximately 1 dB more than the gain of a standard patch antenna.

For the X band beam steering MRAs, the substrate used to build the driven patch antenna is chosen to be Rogers RO4003 which provides good RF characteristics in terms of dielectric permittivity and losses. The parasitic layer uses air as its substrate, where a foam material is used to provide mechanical integrity. Because of the importance of feeding techniques for antenna performance, various types of feeding structures were studied.

There are several basic types of feeding structures including micro-strip feed, coaxial feed, aperture-coupled feed, and coplanar wave guide (CPW). Micro-strip feed and aperture-coupled feed are applied into X band beam steering MRAs. The simulation results indicate that using aperture-coupled micro-strip feed instead of micro-strip inset feed, the common frequency bandwidth increases from 2% to 4%. Also, a larger beam steering angle can be achieved (30^0 vs. 15^0) along with a higher maximum realized gain on all steered beam directions (7.8 dB vs. 5 dB).

As the demand on higher rate data transmission keeps growing, 60 GHz WPAN systems are gaining popularity. Two different MRA designs, which are compatible for the requirements of WPAN, have been introduced. The substrates used for these design are built by bisbenzocyclobutene (BCB). BCB is in liquid form and can be deposited on a support substrate such as quartz by using micro-fabrication techniques. These MRAs operate over two frequency bands 57.24 - 59.4 GHz and 63.72 - 65.88 GHz. One of the designs also provides variable dual polarizations (linear and circular). The MRA designs exhibit reasonably high realized gains ($\sim$7 dB) with the integrity of corresponding radiation patterns maintained over the reconfigurable frequency bands. It is worth mentioning that the dual polarization MRA could shift between linear and circular polarizations with a common frequency bandwidth of 3.33% over the center resonant frequency.

Finally, a beam steering antenna for 60 GHz WPAN is proposed and the basic patch antenna for this application is designed. The substrate for driven patch antenna element is built by SU-8 and the parasitic layer substrate is chosen to be an air layer. SU-8 is a micro-fabrication compatible material with good RF characteristics. It enables the antenna design to be built by using micro-fabrication processes. The initial simulated results for the driven patch antenna element are provided. The antenna resonates at 59.7 GHz with a maximum realized gain of 3.5 dB. As a future work, the results obtained from this work will be used to fabricate MRAs integrated with MEMS and micro-fluidic type switches. As some recent work suggests liquid metals such as Galinstan and Mercury can be used to tune antenna properties, thereby achieving a reconfigurable antenna based on liquid metals [5].

It was shown that the fine control of the movement of the liquid metal within the antenna architecture results in an excellent beam reconfigurability. Figure 7.1(a) and Fig. 7.1(b) show different status of a micro fluidic switch, which also relies on the fine control on the movement of the liquid metal droplet. These types of switches are planned to be used in the future work, which will require not only robust antenna design procedures presented in this thesis work but also high-yield and reliable micro-fabrication processes.

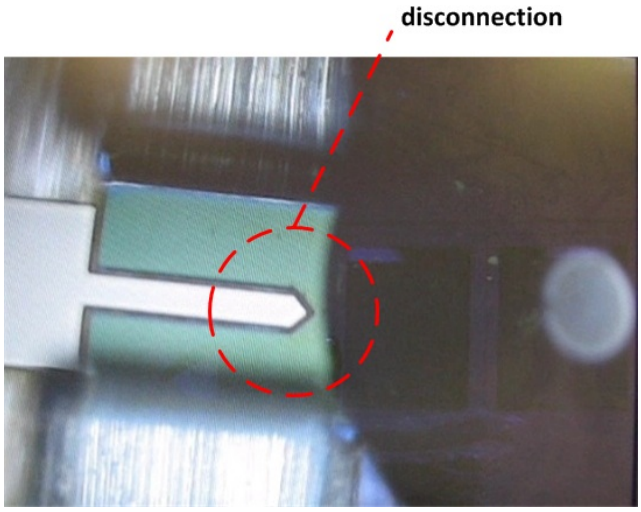

(a)

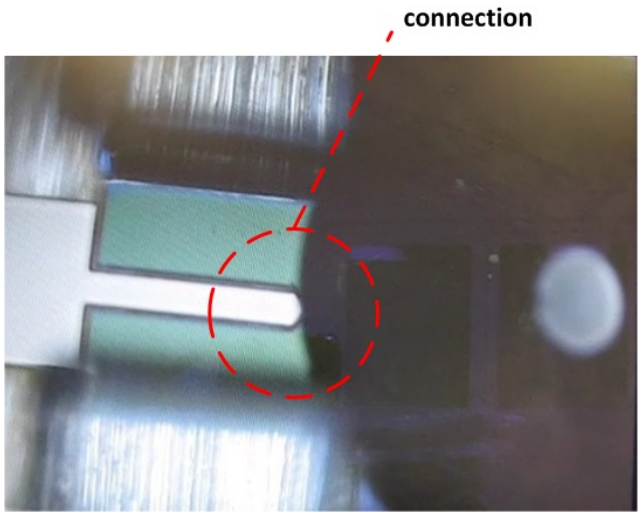

(b)

Fig. 7.1: Schematics of switch status: (a) switch disconnection, and (b) swictch connection.

References

[1] "Special issue on multifunction antennas and antenna systems," *Antennas and Propagation, IEEE Transactions*, vol. 52, p. 2807, Oct. 2004.

[2] B. Cetiner, J. Qian, H. Chang, M. Bachman, G. Li, and F. De Flaviis, "Monolithic integration of rf mems switches with a diversity antenna on pcb substrate," *Microwave Theory and Techniques, IEEE Transactions*, vol. 51, pp. 332–335, Jan. 2003.

[3] L. Pringle, P. Harms, S. Blalock, G. Kiesel, E. Kuster, P. Friederich, R. Prado, J. Morris, and G. Smith, "A reconfigurable aperture antenna based on switched links between electrically small metallic patches," *Antennas and Propagation, IEEE Transactions*, vol. 52, pp. 1434–1445, June 2004.

[4] D. Rodrigo, Y. Damgaci, M. Unlu, L. Jofre, and B. Cetiner, "Small pixelled antenna with mems-reconfigurable radiation pattern," *IEEE International Symposium on Antennas and Propagation and USNC-URSI National Radio Science Meeting*, pp. 1–4, July 2010.

[5] D. Rodrigo, L. Jofre, and B. Cetiner, "Circular beam-steering reconfigurable antenna with liquid metal parasitics," *Antennas and Propagation, IEEE Transactions*, vol. 60, no. 4, pp. 1796–1802, Apr. 2012.

[6] J. Boerman and J. Bernhard, "Performance study of pattern reconfigurable antennas in mimo communication systems," *Antennas and Propagation, IEEE Transactions*, vol. 56, pp. 231–236, Jan. 2008.

[7] S. D. Targonski, R. B. Waterhouse, and D. M. Pozar, "Design of wide-band aperture stacked patch microstrip antennas," *Antennas and Propagation, IEEE Transactions*, vol. 46, pp. 1245–1251, 1998.

[8] N. Behdad and K. Sarabandi, "Dual-band reconfigurable antenna with a very wide tunability range," *Antennas and Propagation, IEEE Transactions*, vol. 54, no. 2, pp. 409–416, Feb. 2006.

[9] H. Eslami, C. Sukumar, D. Rodrigo, S. Mopidevi, A. Eltawil, L. Jofre, and B. Cetiner, "Reduced overhead training for multi reconfigurable antennas with beam-tilting capability," *Wireless Communications, IEEE Transactions*, vol. 9, pp. 3810–3821, Dec. 2010.

[10] J. Petko and D. Werner, "Pareto optimization of thinned planar arrays with elliptical mainbeams and low sidelobe levels," *Antennas and Propagation, IEEE Transactions*, vol. 59, no. 5, pp. 1748–1751, May 2011.

[11] C. Dietrich, J. Bradle, K. Dietze, J. Nealy, and W. Stutzman, "Spatial, polarization, and pattern diversity for wireless handheld terminals," *Antennas and Propagation, IEEE Transactions*, vol. 49, no. 9, pp. 1271–1281, Sept. 2001.

[12] B. Cetiner, H. Jafarkhani, J.-Y. Qian, H. J. Yoo, A. Grau, and F. De Flaviis, "Multifunctional reconfigurable mems integrated antennas for adaptive mimo systems," *Communications Magazine, IEEE Transactions*, vol. 42, pp. 42–70, Dec. 2004.

[13] A. Sayeed and V. Raghavan, "Maximizing mimo capacity in sparse multipath with reconfigurable antenna arrays," *IEEE Journal of Selected Topics in Signal Processing*, vol. 1, pp. 156–166, June 2007.

[14] D. Piazza, N. Kirsch, A. Forenza, R. Heath, and K. Dandekar, "Design and evaluation of a reconfigurable antenna array for mimo systems," *Antennas and Propagation, IEEE Transactions*, vol. 56, pp. 869–881, Mar. 2008.

[15] A. Grau, H. Jafarkhani, and F. De Flaviis, "A reconfigurable multiple-input multiple-output communication system," *Wireless Communications, IEEE Transactions*, vol. 7, pp. 1719–1733, May 2008.

[16] B. Cetiner, E. Akay, E. Sengul, and E. Ayanoglu, "A mimo system with multifunctional reconfigurable antennas," *Antennas and Wireless Propagation Letters, IEEE*, vol. 5, pp. 463–466, Dec. 2006.

[17] S. Catreux, V. Erceg, D. Gesbert, and J. Heath, R.W., "Adaptive modulation and mimo coding for broadband wireless data networks," *Communications Magazine, IEEE Transactions*, vol. 40, pp. 108–115, June 2002.

[18] S. Preston, D. Thiel, T. Smith, S. O'Keefe, and J. W. Lu, "Base-station tracking in mobile communications using a switched parasitic antenna array," *Antennas and Propagation, IEEE Transactions*, vol. 46, pp. 841–844, June 1998.

[19] N. Scott, M. Leonard-Taylor, and R. Vaughan, "Diversity gain from a single-port adaptive antenna using switched parasitic elements illustrated with a wire and monopole prototype," *Antennas and Propagation, IEEE Transactions*, vol. 47, pp. 1066–1070, June 1999.

[20] A. Khaleghi, J. Bolomey, and A. Azoulay, "A pattern diversity antenna with parasitic switching elements for wireless LAN communications," *Wireless Communication Systems 2nd International Symposium*, pp. 611–615, Sept. 2005.

[21] C. won Jung, M. jer Lee, G. Li, and F. De Flaviis, "Reconfigurable scan-beam single-arm spiral antenna integrated with rf-mems switches," *Antennas and Propagation, IEEE Transactions*, vol. 54, no. 2, pp. 455–463, Feb. 2006.

[22] J. Maloney, M. Kesler, L. Lust, L. Pringle, T. Fountain, P. Harms, and G. Smith, "Switched fragmented aperture antennas," *Antennas and Propagation Society International Symposium*, vol. 1, no. 1, pp. 310–313, 2000.

[23] E. Erdil, K. Topalli, M. Unlu, O. Civi, and T. Akin, "Frequency tunable microstrip patch antenna using RF mems technology," *Antennas and Propagation, IEEE Transactions*, vol. 55, no. 4, pp. 1193–1196, Apr. 2007.

[24] R. Mishra, S. Pattnaik, and N. Das, "Tuning of microstrip antenna on ferrite substrate," *Antennas and Propagation, IEEE Transactions*, vol. 41, no. 2, pp. 230–233, Feb. 1993.

[25] J.-C. Chiao, Y. Fu, I. M. Chio, M. DeLisio, and L.-Y. Lin, "Mems reconfigurable vee antenna," *Microwave Symposium Digest, IEEE MTT-S International*, vol. 4, no. 4, pp. 1515–1518, Feb. 1999.

[26] J.-C. Langer, J. Zou, C. Liu, and J. Bernhard, "Micromachined reconfigurable out-of-plane microstrip patch antenna using plastic deformation magnetic actuation," *Microwave and Wireless Components Letters, IEEE*, vol. 13, no. 3, pp. 120–122, Mar. 2003.

[27] J.-C. Chiao, Y. Fu, I. M. Chio, M. DeLisio, and L.-Y. Lin, "Reversibly deformable and mechanically tunable fluidic antennas," *Advanced Functional Materials*, vol. 19, no. 22, pp. 3632–3637, Nov. 2009.

[28] S. Cheng, A. Rydberg, K. Hjort, and Z. Wu, "Liquid metal stretchable unbalanced loop antenna," *Applied Physics Letters*, vol. 94, no. 14, pp. 144–103, Apr. 2009.

[29] R. Harrington, "Reactively controlled directive arrays," *Antennas and Propagation, IEEE Transactions*, vol. 26, pp. 390–395, May 1978.

[30] R. Al-Dahleh, C. Shafai, and L. Shafai, "Frequency-agile microstrip patch antenna using a reconfigurable mems ground plane," *Microwave and Optical Technology Letters*, vol. 43, no. 1, pp. 64–67, Oct. 2004.

[31] D. Pozar and S. Duffy, "A dual-band circularly polarized aperture-coupled stacked microstrip antenna for global positioning satellite," *Antennas and Propagation, IEEE Transactions*, vol. 45, no. 11, pp. 1618–1625, Nov. 1997.

[32] L. Economou and R. Langley, "Dual band hybrid vehicular telephone antenna," *Microwaves, Antennas and Propagation, IEE Proceedings*, vol. 149, no. 1, pp. 41–44, Feb. 2002.

[33] W. Weedon, W. Payne, and G. Rebeiz, "Mems-switched reconfigurable antennas," *Antennas and Propagation Society International Symposium*, vol. 3, no. 3, pp. 654–657, 2001.

[34] J. R. James and P. S. Hall, *Handbook of Microstrip Antennas*. London, UK: Peter Peregrinus, 1989.

[35] Y. Kuwahara, "Multiobjective optimization design of yagi-uda antenna," *Antennas and Propagation, IEEE Transactions*, vol. 53, no. 6, pp. 1984–1992, June 2005.

[36] C. Li and Q. Feng, "Multi-objective optimization design of multilayer rfid tag antenna by pareto ga," *Microwave and Millimeter Wave Technology (ICMMT)*, pp. 32–35, May 2010.

[37] C. van Coevorden, S. Garcia, M. Pantoja, A. Bretones, and R. Martin, "Microstrip-patch array design using a multiobjective ga," *Antennas and Wireless Propagation Letters, IEEE*, vol. 4, pp. 100–103, June 2005.

[38] J. Petko and D. Werner, "The pareto optimization of ultrawideband polyfractal arrays," *Antennas and Propagation, IEEE Transactions*, vol. 56, no. 1, pp. 97–107, Jan. 2008.

[39] S. Fisher, D. Weile, E. Michielssen, and W. Woody, "Pareto genetic algorithm based optimization of log-periodic monopole arrays mounted on realistic platforms," *Electromagnetic Waves and Applications,*, vol. 13, no. 5, pp. 571–598, 1995.

[40] D. Boeringer and D. Werner, "Bezier representations for the multiobjective optimization of conformal array amplitude weights," *Antennas and Propagation, IEEE Transactions*, vol. 54, no. 7, pp. 1964–1970, July 2006.

[41] S. K. Goudos, Z. D. Zaharis, M. Salazar-Lechuga, P. I. Lazaridis, and P. B. Gallion, "Dielectric filter optimal design suitable for microwave communications by using multi-objective evolutionary algorithms," *Microwave And Optical Technology Letters*, vol. 49, no. 10, pp. 2324–2329, Oct. 2007.

[42] D. Weile, E. Michielssen, and D. Goldberg, "Genetic algorithm design of pareto optimal broadband microwave absorbers," *Electromagnetic Compatibility*, vol. 38, no. 3, pp. 518–525, Aug. 1996.

[43] S. Cui, A. Mohan, and D. Weile, "Pareto optimal design of absorbers using a parallel elitist nondominated sorting genetic algorithm and the finite element-boundary integral method," *Antennas and Propagation, IEEE Transactions*, vol. 53, no. 6, pp. 2099–2107, June 2005.

[44] L. Jiang, J. Cui, L. Shi, and X. Li, "Pareto optimal design of multilayer microwave absorbers for wide-angle incidence using genetic algorithms," *Microwaves, Antennas and Propagation, IET*, vol. 3, no. 4, pp. 572–579, June 2009.

[45] H. Choo, H. Ling, and C. Liang, "On a class of planar absorbers with periodic square resistive patches," *Antennas and Propagation, IEEE Transactions*, vol. 56, no. 7, pp. 2127–2130, July 2008.

[46] Ansoft HFSS, [www.ansoft.com], 2011.

[47] G. M. Rebeiz, *RF MEMS: Theory, Design, and Technology.* New York: Wiley-Interscience, 2002.

[48] Y. J. Lee, J. Yeo, R. Mittra, and W. S. Park, "Application of electromagnetic bandgap (ebg) superstrates with controllable defects for a class of patch antennas as spatial angular filters," *Antennas and Propagation, IEEE Transactions*, vol. 23, pp. 224–235, Jan. 2005.

[49] J. Audren and P. Brault, "High frequency antenna with a variable direction radiation pattern," U.S. Patent 5,235,343, Aug. 10, 1993.

[50] J. Cheng, M. Hashiguchi, K. Iigusa, and T. Ohira, "Electronically steerable parasitic array radiator antenna for omni- and sector pattern forming applications to wireless ad hoc networks," *Microwaves, Antennas and Propagation, IEE Proceedings*, vol. 105, pp. 203–208, Aug. 2003.

[51] Synthetic Quartz Glass Substrates, Shin-Etsu Chemical CO., Ltd, [http://www.shinetsu.co.jp/e/product/pdf/garasu.pdf], 2009.

[52] D. V. Thiel and S. Smith, *Switched Parasitic Antennas for Cellular Communications*. Norwood, MA: Artech House, 2002.

[53] J. Huang, "Planar microstrip yagi array antenna," *Antennas and Propagation Society International Symposium, AP-S. Digest*, pp. 894–897, June 1989.

[54] D. Pozar, "Input impedance and mutual coupling of rectangular microstrip antennas," *Antennas and Propagation, IEEE Transactions*, vol. 30, pp. 1191–1196, Nov. 1982.

[55] L. Diaz and T. Milligan, *Antenna Engineering Using Physical Optics*. Norwood, MA: Artech House, 1996.

[56] K. F. Lee and W. Chen, *Advances in Microstrip and Printed Antennas*. New York: John Wiley and Sons, 1997.

[57] F. Yang and Y. Rahmat-Samii, *Electromagnetic Band Gap Structures in Antenna Engineering*. New York: Cambridge University Press, 2009.

[58] S. Ramo, J. R. Whinnery, and T. V. Duzer, *Fields and Waves in Communication Electronics*, 2nd ed. New York: Wiley, 1984.

[59] D. Pozar, "Surface wave effects for millimeter wave printed antennas," *Antennas and Propagation Society International Symposium*, pp. 692–695, Jan. 2003.

[60] D. Sievenpiper, L. Zhang, R. Broas, N. Alexopolous, and E. Yablonovitch, "High-impedance electromagnetic surfaces with a forbidden frequency band," *Microwave Theory and Techniques, IEEE Transactions*, vol. 47, pp. 2059–2074, Nov. 1999.

[61] R. Coccioli, F.-R. Yang, K.-P. Ma, and T. Itoh, "Aperture-coupled patch antenna on uc-pbg substrate," *Microwave Theory and Techniques, IEEE Transactions*, vol. 47, pp. 2123–2130, Nov. 1999.

[62] A. Al-Zoubi, F. Yang, and A. Kishk, "A low-profile dual-band surface wave antenna with a monopole-like pattern," *Antennas and Propagation, IEEE Transactions*, vol. 55, pp. 3404–3412, Dec. 2007.

[63] N. Srinivas and K. Deb, "Muiltiobjective optimization using nondominated sorting in genetic algorithms," *Evolutionary Computation*, vol. 2, pp. 221–248, Fall 1994.

[64] K. Deb, A. Pratap, S. Agarwal, and T. Meyarivan, "A fast and elitist multiobjective genetic algorithm: Nsga-ii," *Evolutionary Computation, IEEE Transactions*, vol. 6, no. 2, pp. 182–197, Apr. 2002.

[65] Matlab, [www.mathworks,com], 2009.

[66] J. R. James, P. S. Hall, and C. Wood, *Microstrip Antennas: Theory and Design*. London, UK: Peter Peregrinus, 1981.

[67] P. Bharitia, K. V. S. Rao, and R. S. Tomar, *Millimeter-Wave Microstrip and Printed Circuit Antennas*. Norwood, MA: Artech House, 1991.

[68] D. M. Pozar, "Microstrip antennas," *Proceedings IEEE*, vol. 80, pp. 79–91, 1992.

[69] R. Garg, P. Bhartia, I. Bahl, and A. Ittipiboon, *Microstrip Antenna Design Handbook*. Norwood, MA: Artech House, 2001.

[70] K. C. Gupta, *Microstrip Lines and Slot Lines*, 2nd ed. Norwood, MA: Artech House, 1996.

[71] W. Menzel and W. Grabherr, "A microstrip patch antenna with coplanar line feed," *Microwave and Guided Wave Letters, IEEE*, vol. 1, pp. 340–342, 1991.

[72] R. Smith and J. T. Williams, "Coplanar waveguide feed for microstrip patch antennas," *Electronics Letters*, vol. 28, pp. 2272–2274, 1992.

[73] D. M. Pozar and D. H. Schaubert, *The Analysis and Design of Microstrip Antennas and Arrays*. New York: Wiley-IEEE Press, 1995.

[74] A. W. Scott and R. Frobenius, *RF Measurements for Cellular Phones and Wireless Data Systems*. Hoboken, NJ: John Wiley & Sons, Inc., 2008.

Appendices

Appendix A

Feeding Techniques and Modeling

Micro-strip antennas have radiating elements on one side of a dielectric substrate, and thus early micro-strip antennas were fed either by a micro-strip line or a coaxial probe through the ground plane. Since then a number of new feeding techniques have been developed. Prominent among these are micro-strip feed, coplanar waveguide feed, aperture-coupled micro-strip feed [34, 66–68].

Selection of the feeding technique is governed by a number of factors. The most important consideration is the efficient transfer of power between the radiating structure and feed structure, that is, impedance matching between the two. Associated with impedance matching are stepped impedance transformers, bends, stubs, junctions, transitions, and so on, which introduce discontinuities leading to spurious radiation and surface wave loss. The undesired radiation may increase the side lobe level and the cross-polar amplitude of the radiation pattern. Minimization of spurious radiation and its effect on the radiation pattern is one of the important factors for the evaluation of the feed. Another consideration is the suitability of the feed for array applications. Some feed structures are amenable to better performance because of the larger number of parameters available [69].

A.1 Micro-strip Feed

Excitation of the micro-strip antenna by a micro-strip line on the same substrate appears to be a natural choice because the patch can be considered an extension of the micro-strip line, and both can be fabricated simultaneously. But this techique has some limitations. The edge-coupled feed suffers from a limitation of impedance mismatch because the input impedance of the feed line. Therefore, an external impedance matching circuit is used between the patch edge and the 50Ω micro-strip line. The impedacne matching cir-

cuit, beside giving rise to spurious radiation, cannot be accommodated in arrays, because of the nonavailability of physical space on the substrate. The micro-strip line blocks radiation from the portion of the patch with which it is in contact resulting in reduced radiation. This is a serious limitation of this feed at millimeter-wave frequencies where the patch width can be comparable to the width of the micro-strip line.

An improvement of the coplanar feed that overcomes some of the shortcomings is that micro-strip line is inset into the patch. The feed position is selected such that the input impedance of the antenna is 50Ω.

Micro-strip feeds are easy to design and fabricate. However, feed micro-strip lines contribute to spurious radiation. Therefore, they have been used in applications where teh demand on performance is not too stringent and the feed must be coplanar with the patch. The bandwidth achieved is 3% to 5%.

A.2 Coplanar Waveguide Feed

A coplanar waveguide (CPW) is the preferred transmission line for microwave monolithic integrated circuits (MMICs) [70]. Both the CPW and micro-strip antennas belong to the planar geometry. Therefore, for integrating micro-strip antennas with MMICs, it is desirable to feed the micro-strip antennas with a CPW [71, 72]. The CPW is etched in the ground plane of the micro-strip antenna. Coupling is accomplished via a slot.

An advantage of a CPW feed is that the radiation from the feed structure is negligible because the coplanar waveguide is excited in the odd mode of the coupled slot line [70]. Due to this mode, the equivalent magnetic currents on both the CPW slots radiate almost out of phase, contributing negligibly to the feed radiation. This feature of a CPW feed is useful in the design of antenna arrays since mutual coupling between adjacent lines is minimized.

A.3 Aperture-Coupled Micro-strip Feed

The notable features of this feed configuration [73] are wider bandwidth, and the shielding of the radiating patch from the radiation emanating from the feed structure. The basic structure uses two substrates separated by a common ground plane. A micro-strip feed line

on the lower substrate is electromagnetically coupled to the patch through a slot aperture in the common ground plane. The slot can be of any shape or size, and these parameters can be used to improve the bandwidth. The substrate parameters for the two layers are chosen in a manner to optimize the feed and radiation functions independently. For example, the substrate for the feed line should be thin and of high dielectric constant, whereas the substrate for the patch can be thick and of lower dielectric constant. Moreover, radiation from the open end of the feed line does not interfere with the radiation pattern of the patch because of the shielding effect of the ground plane. This feature also improves the polarization purity. If the coupling slot is non-resonant, the back lobe radiation from the slot is typically 15 to 20 dB below the forward main beam.

The coupling slot is nearly centered with respect to the patch where the magnetic field of the patch is maximal. This is done purposely to enhance magnetic coupling between the magnetic field of the patch and the equivalent magnetic current near the slot.

In addition to the merits of the feeding technique described above, this feed can be designed to improve bandwidth by adjusting the shape and length of the coupling slot, width of the feed line, and stub length. An impedance bandwidth of about 21% has been reported for an unstacked patch [7].

Appendix B

Antenna Measurement Equipments

Testing of antennas are required to ensure that the antenna meets specifications or simply to characterize. There are some basic RF measurement equipments introduced here.

B.1 Vector Network Analyzer (VNA)

An RF VNA measures the response of both RF devices and networks (which is a group of devices) as a function of the frequency of an applied continuous, non-modulated, RF signal [74]. The VNA measures the response of the network one frequency at a time, but it varies the measurement frequency over the user adjusted RF bandwidth very rapidly, making hundreds of measurement in 1 s.

The term vector designates the fact that the VNA measures both the amplitude and phase of the RF signal.

The VNA measures the incident test signal, the reflected test signal, and the transmitted signal from the RF devices. Then it automatically reverses the connections to measure the same quantities looking into the device from the opposite direction. The VNA can display these measured quantities as a function of frequency. However, it usually processes the information first to display derived quantities such as return loss, insertion loss, scattering parameters (S-parameters) in amplitude and phase, Smith Charts, group delay, and other performance characteristics.

For radio measurements, such as return loss or insertion loss, where two power levels are being compared to each other, the VNA's measurement accuracy can be improved to 0.1 dB or better by first calibrating the VNA to a set of standards, usually a short, open, load, and through. This calibration can be done manually by the operator, which eliminates operator error and also protects the standards from handing damage.

B.2 Spectrum Analyzers

Spectrum analyzers can measure all of the individual frequencies that exist in any particular RF signal and display the power level of each frequency separately.

Note the difference between a spectrum analyzer and a VNA. The VNA analyzers the performance of a single RF device or combination of devices, either of which is called a "network." It measures the performance of the network one frequency at a time. The spectrum analyzer analyzes a signal to describe the power of each of the frequencies that make up the signal. The spectrum analyzer may be used to measure the distortion that the RF device creates on the different frequency components of the signal passing through it.

B.3 Antennas

Specifications for antenna are following: gain, beam width, pattern, polarization, and impedance match. Gain is a measure in dB of how well the antenna concentrates the power in the direction of the receiver, relative to an isotropic antenna. An isotropic antenna is defined as an idealized antenna that radiates power equally in all directions. Beam width is the angular width of the beam generated by the antenna. Gain and beam width are related. To achieve more gain, the width of the beam must be decreased.

The antenna pattern defines radiation in undesired directions that may jam other systems. Polarization defines the direction of the electric field of the radiation, whether directed vertically or horizontally to the Earth's surface. Every antenna serves as an impedance transformer, transforming the impedance of the antenna at its RF connector to 50 or 75Ω.

The properties of the antennas can be measured easily using a VNA, which can measure the input power to the antenna and the output power received from the antenna about 10 wavelengths away in the far field region and then calculate the gain. If the antenna is mounted on a rotating platform, its antenna pattern can be measured. The one requirement for all of these measurements is that they be made in an anechoic test room, which has absorbing material mounted on its walls, floors, and ceiling so that no reflected signal degrades the measurement results.

Vita

Xiaoyan Yuan

Published Journal Articles

- A Parasitic Layer-Based Reconfigurable Antenna Design by Multi-Objective Optimization, X. Yuan*, Z. Li, H. Mopidevi, O. Kaynar and Bedri A. Cetiner, *IEEE Trans. Antennas Propagation, June 2011.*

Published Conference Papers

- Full-wave analysis of 60 GHz reconfigurable antenna for WPAN applications, X. Yuan*, Y. Damgaci, and B. A. Cetiner, in *Progress in Electromagnetic Research Symposium (PIERS)*, 2010.

- RF-N/MEMS Integrated Reconfigurable Antenna for Public Safety Applications, X. Yuan*, Y. Damgaci, H. Mopidevi and B.A. Cetiner, in *IEEE International Symposium on Antennas Propagation*, Jan. 2009.

- RF-Nems Integrated Frequency Reconfigurable Antenna for Waveform Diversity Schemes, Yasin. Damgaci, Xiaoyan. Yuan, Necmi Biyikli, Bedri A. Cetiner, *USNC-URSI National Radio Science Meeting*, Jan. 2009.